



# CHORUS

This is the accepted manuscript made available via CHORUS. The article has been published as:

## Extending comb-based spectral estimation to multiaxis quantum noise

Gerardo A. Paz-Silva, Leigh M. Norris, Félix Beaudoin, and Lorenza Viola

Phys. Rev. A **100**, 042334 — Published 31 October 2019

DOI: [10.1103/PhysRevA.100.042334](https://doi.org/10.1103/PhysRevA.100.042334)

# Extending comb-based spectral estimation to multi-axis quantum noise

Gerardo A. Paz-Silva,<sup>1,\*</sup> Leigh M. Norris,<sup>2,\*</sup> Félix Beaudoin,<sup>2,3</sup> and Lorenza Viola<sup>2</sup>

<sup>1</sup>*Centre for Quantum Dynamics & Centre for Quantum Computation and Communication Technology, Griffith University, Brisbane, Queensland 4111, Australia*

<sup>2</sup>*Department of Physics and Astronomy, Dartmouth College, 6127 Wilder Laboratory, Hanover, New Hampshire 03755, USA*

<sup>3</sup>*NanoAcademic Technologies, 666 rue Sherbrooke Ouest, Suite 802, Montréal, Québec, Canada H3A 1E7*

(Dated: September 23, 2019)

We show how to achieve full spectral characterization of general multi-axis additive noise on a single qubit, including arbitrary cross-axis **noise** correlations. Our pulsed spectral estimation technique is based on sequence repetition and frequency-comb sampling and is applicable in principle even to models where a large qubit energy-splitting is present, as long as the noise is stationary and a second-order (Gaussian) approximation to the controlled reduced dynamics is viable. A key innovation in our approach is a spherical representation of the noise in terms of operators that couple directly to raising/lowering qubit operators, which is instrumental to show that only three suitably defined spectra effectively contribute in the large-splitting regime. Our result is crucial to extend the applicability of comb-based spectral estimation, which has been so far employed under the assumption of dephasing-dominated dynamics, to experimental platforms where both  $T_1$  and  $T_2$  processes may occur on comparable time scales or be otherwise significant, such as superconducting qubits.

## I. INTRODUCTION

Improving the coherence properties of quantum systems in the presence of unwanted noise is a key step toward realizing the full potential of quantum technologies [1]. In particular, obtaining a quantitatively accurate characterization of noise is instrumental to validate theoretical modeling and prediction as well as to design physical-layer quantum control strategies that are optimally tailored to realistic time-dependent noise environments. Acquiring this knowledge is the overarching goal of *quantum noise spectroscopy* (QNS), a body of techniques through which noise spectra or correlation functions are estimated based on measurements of dynamical observables of the quantum system of interest (a single qubit sensor in the simplest case) under appropriately chosen external controls and measurements [2–8]. In conjunction with algorithmic error mitigation that can be achieved through proper quantum-circuit design and compiling [9, 10], spectral properties inferred from QNS are expected to play an important role in enabling near-term intermediate-scale quantum information processors [11]. Ultimately, directly probing the behavior of noise correlations through multiqubit QNS may prove crucial in determining the viability of large-scale fault-tolerant quantum computation [12] and in overcoming the effect of correlated quantum noise in entanglement-assisted metrology [13].

In recent years, a large focus of QNS has been on characterizing *dephasing noise*, that is, noise that couples exclusively along the system’s quantization axis and results in transverse relaxation (“ $T_2$  effects”). **Contributions of additional, off-axis noise sources resulting in longitudinal relaxation (“ $T_1$  effects”)** have either been assumed to be *a priori* negligible or accommodated to a limited extent – within *ad hoc*, phenomenological models by invoking extra assumptions on the noise functional form or degree of tunability [14, 15], or approaches requiring access to full quantum process tomogra-

phy [16]. Likewise, correlations between noise across different axes have been partially characterized in a tunable flux qubit in *parametric* form, by assuming a  $1/f$  frequency dependence for all the spectra [17]. As a result, most QNS protocols to date involve *single-axis spectral estimation*. These methods have been developed and implemented following two main paradigms: multipulse approaches inspired by dynamical decoupling (DD), in which control sequences consisting of nearly-instantaneous pulses are applied [2, 3, 18, 19]; and continuous-wave (CW) approaches inspired by “spin-locking” relaxometry [14, 20, 21], in which the control is, typically, a resonant radio-frequency or microwave drive with constant amplitude and noise is probed during driven evolution. In both cases, the basic idea is to shape the control modulation so that the frequency response of the driven qubit sensor is altered in a desired way [22]. To date, experimental application of QNS has enabled successful reconstructions of dephasing noise spectra in physical settings as diverse as nuclear magnetic resonance [3, 21], superconducting qubits [2, 23], spin qubits in semiconductors [24–26], trapped ions [27, 28], and NV centers in diamond [29, 30]. QNS protocols for high-order dephasing spectra resulting from non-Gaussian statistics have also been validated experimentally, using engineered noise on a superconducting qubit sensor operated outside of a linear-response regime [31].

The assumption of single-axis noise processes is too restrictive from both a conceptual and a practical standpoint, however. Many superconducting qubits, for instance, operate in a regime far from pure dephasing, in which the  $T_1$  and  $T_2$  time scales due to natural noise processes may be of the same order of magnitude [32–34]. In addition, recent advances with spin qubits in semiconductors [35, 36] have relied on hybridizing spin and charge degrees of freedom by exploiting exchange-based interactions or the inhomogeneous magnetic field from a micro-magnet, thereby exposing the logical qubit to both longitudinal and transverse noise due to electric fluctuations or coupling to phonons [35, 37–39]. Since noise along distinct qubit axes may a priori arise from the same physical source (e.g., two-level fluctuators or phonons), the corre-

---

\* These authors contributed equally to this work.

sponding noise processes need not be uncorrelated. Therefore, a complete characterization of noise processes does not only require the *simultaneous reconstruction* of the noise spectra along *all* relevant qubit axes, but also mandates the estimation of cross-correlation spectra *between* different noise axes.

In this work, we tackle the problem of *multiaxis spectral estimation*, by allowing a single qubit sensor to be exposed to general quantum noise with arbitrary correlations along all three axes of the Bloch sphere. Specifically, in the context of DD-based QNS, we focus on non-parametric spectral estimation by *frequency-comb* techniques, as introduced by Alvarez and Suter [3]. The basic idea, in the simplest setting of a stationary Gaussian dephasing noise process described by a power spectral density (PSD)  $S(\omega)$ , is that repetition of a sufficiently large number  $M \gg 1$  of a “base” pulse sequence with duration  $T_c$  effectively shapes the filter function (FF) that describes the control modulation in frequency space into a frequency comb with narrow teeth. This enables  $S(\omega)$  to be sampled over a frequency grid determined by the harmonics,  $\omega_m \equiv m(2\pi/T_c)$ , with  $m \in \mathbb{Z}$ . Aside from its conceptual appeal, comb-based QNS affords a number of advantages. Unlike CW approaches, no weak-coupling approximations are needed, for either a single qubit or multiple qubits, as long as the noise is dephasing and Gaussian, which has enabled theoretical extensions to multiqubit settings – including access to non-classical (asymmetric) spectra and spatio-temporal harmonic features [40–42]. The fact that sequence repetition also enforces the emergence of a comb structure in all FFs relevant to high-order dephasing spectra offers a direct means to probe non-Gaussian classical as well as quantum bosonic environments [6, 43]. Lastly, compared to other DD-based techniques, such as  $N$ -pulse Carr-Purcell-Meiboom-Gill spectroscopy [2], the frequency-comb approach is less susceptible to spectral leakage [5], since it takes higher-order harmonics into account in principle.

In practice, comb-based QNS approaches also face limitations in the presence of realistic timing constraints and non-idealities in control and measurements. For instance, deviations from the ideal frequency comb approximation due to finite number of repetitions may bias or significantly complicate the spectral reconstruction procedure, although some compensation may be possible at the cost of additional measurements and analysis [44]. Most importantly for the present discussion, since the resolution to which the PSD may be sampled is determined by the duration  $T_c$  of the base sequence, increasing  $T_c$  is the only way to obtain a finer sampling grid, with no additional “knob” available to independently tune the maximum range of the reconstruction [5]. This may lead to a large inversion problem, making the approach vulnerable to ill-conditioning and to the numerical errors that follow. Even if numerical stability may be improved by employing suitable regularization [31], use of long evolution times for increased sampling resolution may be incompatible with a pure-dephasing approximation for many systems of interest.

With the above considerations in mind, our main objective here is to determine whether and how comb-based QNS may be extended to the characterization of stationary multi-axis single-qubit noise and, if so, to further understand ap-

plicability and limitations in realistic scenarios. To answer these questions, we find it useful to contrast a “driftless” setting – in which the qubit energy splitting  $\Omega = 0$  and thus no internal qubit dynamics is present – to one where the qubit energy splitting  $\Omega \neq 0$  and cannot be neglected. Even if we assume noise to be Gaussian, both situations require perturbative methods, unlike for comb-based QNS in a pure-dephasing setting. Nonetheless, assuming the time-ordered (Dyson) cumulant expansion that determines expectation values of time-evolved qubit observables may indeed be truncated to the second (Gaussian) order, we find that in the driftless setting, complete reconstruction of *all* multiaxis spectra is possible – including both classical and quantum spectra, the latter arising from non-commuting noise operators. For arbitrary non-zero qubit energy splitting, all of the spectra can still be reconstructed, in principle, by imposing a *synchronization constraint* between the internal and the control dynamics, namely,  $\Omega T_c = 2\pi k$ , with  $k \in \mathbb{Z}$ . While such a constraint can be hard to meet in practice for realistically large values of  $\Omega$ , we show that in precisely this case drastic simplifications occur, provided that  $\Omega T \gg 1$ , with  $T = MT_c$  being the total evolution time. Indeed, in this regime, the contribution of most of the multiaxis spectra becomes negligible, and the reduced qubit dynamics is effectively *characterized by only three spectra*: one dephasing spectrum, determined by the two-point autocorrelation of noise operators along the quantization axis (say,  $z$ ), and two generally complex spectra, that result from two-point correlators of off-axis noise (along  $x, y$ ). All non-vanishing spectra can be reconstructed using our multiaxis comb-based approach, in principle.

The content is organized as follows. In Sec. II, we describe the relevant open-system model Hamiltonian for the driven single-qubit sensor. In particular, in addition to the standard representation of multiaxis additive noise in terms of Cartesian components, we introduce a *spherical representation* (Sec. II A), which will be expedient for analyzing QNS in the distinctive dynamical regimes mentioned above. We also describe the available pulse control capabilities (Sec. II B), and give the solution for the reduced qubit dynamics within a cumulant expansion truncated to the second order (Sec. II C). In Sec. III, we introduce the noise spectra and the control FFs that are needed for formulating the multiaxis estimation problem in the frequency domain (Sec. III A), and specify the main steps involved in the frequency-comb QNS approach along with the required control symmetries (Sec. III B). Notably, by borrowing from control techniques for decoupled systems [45], we also introduce *frame-tilting control sequences* (Sec. III C), which will be instrumental to achieve the level of flexibility needed for simultaneous multi-spectral reconstruction. In Sec. IV, we provide expressions for the experimentally accessible physical quantities in terms of noise cumulants (Sec. IV A), and show how the distinction between two types of FFs, which we term *balanced* and *imbalanced*, is key for devising QNS protocols in the two distinctive energy-splitting regimes (Sec. IV B). In Sec. V, we further explain how to combine experimental measurements and build control sequences to grant access to all the target spectra, and provide an illustrative example of a numerical reconstruction

(Sec. VB). Section VI is devoted to a critical assessment of comb-based QNS methods in the presence of noise supported over a wide frequency band, pointing to more stringent practical limitations in multi-axis as opposed to single-axis settings for many realistic qubit devices.

## II. SYSTEM AND CONTROL SETTING

### A. Open-system model Hamiltonian

We consider a single qubit interacting with an arbitrary environment (or “bath”) in the presence of open-loop control. In the laboratory frame, the evolution in the joint Hilbert space  $\mathcal{H}_S \otimes \mathcal{H}_B$  is ruled by a total Hamiltonian of the form

$$H_{\text{tot}}^{\text{lab}}(t) = H_S + H_B + H_{SB}(t) + H_{\text{ctrl}}^{\text{lab}}(t),$$

where  $H_S$  ( $H_B$ ) dictates the internal system (bath) free dynamics,  $H_{SB}(t)$  describes the system-bath interaction, and the control Hamiltonian  $H_{\text{ctrl}}^{\text{lab}}(t)$  acts non-trivially only on  $\mathcal{H}_S$ . We will work in the basis in which the qubit Hamiltonian is diagonal, and associate the quantization direction with the  $\sigma_z$  Pauli matrix. In this way, in units  $\hbar = 1$ , the internal system dynamics and the system-bath interaction are described, respectively, by Hamiltonians

$$H_S = \frac{\Omega}{2}\sigma_z, \quad H_{SB}(t) = \sum_{\alpha=x,y,z} \sigma_\alpha \otimes B_\alpha^0(t), \quad (1)$$

where  $\Omega$  is the (known) qubit energy splitting, and  $B_\alpha^0(t) = B_\alpha^{0\dagger}(t)$ , for all  $t$ , are time-dependent bath operators. Note that in writing Eq. (1), we assume that  $\text{tr}_S[H_{SB}(t)] = 0$ , that is, a purely rank-2 coupling [41], [46].

Physically, the bath operators  $B_\alpha^0(t)$  are responsible for introducing noise effects in the reduced qubit dynamics, in a way that will be made quantitatively precise in Sec. IIC. We remark that the definition of what constitutes a transverse (dephasing) vs. a longitudinal (relaxation) decoherence process is tied to the choice of the working frame. Relative to the qubit ( $z$ ) eigenbasis, environmental modes that couple “on-axis” in an energy-conserving fashion contribute only to the transverse relaxation time,  $T_2$ , whereas “off-axis” couplings along  $x, y$  are responsible for both an energy-non-conserving contribution to  $T_2$ , and a finite longitudinal relaxation time,  $T_1$ . If the quantization axis is changed, however, as in spin-locking QNS [20], an originally purely transverse contribution may induce both dephasing and relaxation in the new frame.

In the interaction picture ( $I$ ) with respect to the total internal Hamiltonian  $H_S + H_B$ , the qubit-bath dynamics are generated by

$$H_I(t) = \sum_{\alpha=x,y,z} \sigma_\alpha(t) \otimes B_\alpha(t) + H_{\text{ctrl}}(t),$$

where

$$\begin{aligned} \sigma_\alpha(t) &\equiv e^{i\Omega t\sigma_z/2} \sigma_\alpha e^{-i\Omega t\sigma_z/2}, \\ B_\alpha(t) &\equiv e^{iH_B t} B_\alpha^0(t) e^{-iH_B t} \\ H_{\text{ctrl}}(t) &\equiv e^{i\Omega t\sigma_z/2} H_{\text{ctrl}}^{\text{lab}}(t) e^{-i\Omega t\sigma_z/2}. \end{aligned}$$

Formally, we allow for the bath operators to have both a quantum (non-commuting) and a classical (c-number) component, namely,  $B_\alpha(t) \equiv \bar{B}_\alpha(t) + \zeta_\alpha(t)I_B$ , with  $I_B$  being the bath identity operator and  $\zeta_\alpha(t)$  denoting a classical stochastic process. Thus, the limit of purely classical noise corresponds to  $B_\alpha(t) = \zeta_\alpha(t)I_B$ . In the “driftless” setting when  $\Omega = 0$ , the interaction Hamiltonian reduces to

$$H_I^{(\Omega=0)}(t) = \sum_{\alpha=x,y,z} \sigma_\alpha \otimes B_\alpha(t) + H_{\text{ctrl}}(t). \quad (2)$$

When  $\Omega \neq 0$ , on the other hand, the off-axis couplings induce transitions between the  $\pm\Omega$  qubit eigenstates. In this case, it is convenient to re-express the interaction Hamiltonian in terms of ladder operators,

$$H_I(t) = \sum_{j=-1,0,+1} \sigma_j \otimes e^{ij\Omega t} B_{-j}(t) + H_{\text{ctrl}}(t), \quad (3)$$

where we use the standard quantum-mechanical definition of spherical (rank-1) vector-operator components,

$$v_{\pm 1}(t) \equiv \frac{v_x(t) \pm iv_y(t)}{\sqrt{2}}, \quad v_0(t) \equiv v_z(t).$$

In what follows, as we set up the QNS problem, we will make reference to both the driftless, Cartesian representation in Eq. (2) and the spherical representation in Eq. (3). While doing so may seem excessive at first, we will see later on that different representations facilitate the analysis in different regimes of interest. Accordingly, from here on, we shall use **Greek indices ( $\alpha, \beta$ ) when specifically working in Cartesian coordinates, Latin indices ( $j, l$ ) to specifically denote spherical coordinates, and ( $a, b$ ) when equations apply to both cases.**

### B. Control resources

In order to more easily formulate and analyze the control problem, as customary we further transform the Hamiltonian in Eq. (3) (or the simpler version in Eq. (2)) to the toggling-frame, that is, the interaction picture defined by  $H_{\text{ctrl}}(t)$ , which leads to a Hamiltonian of the form

$$H(t) = \begin{cases} \sum_{\alpha,\alpha'=x,y,z} y_{\alpha,\alpha'}(t) \sigma_{\alpha'} B_\alpha(t) & \text{(Cartesian),} \\ \sum_{j,j'=-1,0,+1} y_{j,j'}(t) e^{ij\Omega t} \sigma_{j'} B_{-j}(t) & \text{(spherical).} \end{cases} \quad (4)$$

Here, following [41, 43], the  $y_{\alpha,\alpha'}(t)$  ( $y_{j,j'}(t)$ ) are switching functions which encapsulate the effect of the applied control in the Cartesian (respectively, spherical) coordinates. Letting  $U_{\text{ctrl}}(t) \equiv \mathcal{T} e^{-i \int_0^t ds H_{\text{ctrl}}(s)}$  denote the time-ordered unitary control propagator, the switching functions are given by

$$y_{a,a'}(t) = \frac{1}{2} \text{tr}[U_{\text{ctrl}}^\dagger(t) \sigma_a U_{\text{ctrl}}(t) \sigma_{a'}^\dagger].$$

Note that the  $y_{\alpha,\alpha'}(t)$  are real, whereas the  $y_{j,j'}(t)$  are generally complex since  $\sigma_{\pm 1}(t)$  are not Hermitian. It is also in-

interesting to note that, for  $j = \pm 1$  in Eq. (4), the corresponding switching functions are effectively multiplied by the time-dependent factor  $e^{\pm i\Omega t}$ ; as we will see, this will have the effect of displacing FFs by  $\pm\Omega$  in the frequency domain.

While the formalism we employ to model the qubit dynamics applies to arbitrary open-loop control, the QNS protocol we will present requires a control Hamiltonian capable of generating arbitrary instantaneous qubit rotations,  $R(\vec{\theta}) \in \text{SO}(3)$ , at pulse times of our choice. By using the parametrization  $R(\vec{\theta}) = R(\theta_x, \theta_y, \theta_z) = R_x(\theta_x)R_y(\theta_y)R_z(\theta_z)$ , we denote the corresponding control pulse by

$$P_{\vec{\theta}} \equiv e^{-i\sigma_x\theta_x/2}e^{-i\sigma_y\theta_y/2}e^{-i\sigma_z\theta_z/2} \in \text{SU}(2). \quad (5)$$

We point out that this parametrization is a matter of generality and should not be taken to require the execution of three individual pulses; indeed, the sample execution of our protocol to be presented in Sec. V will employ only pulses along a single coordinate axis. The action of pulses  $P_{\vec{\theta}}$  on operators in our two bases of interest can be obtained by making use of standard algebraic Pauli identities – in particular,  $\sigma_\alpha\sigma_{\alpha'} = \delta_{\alpha,\alpha'}I_S + i\epsilon_{\alpha\alpha'\beta}\sigma_\beta$  and  $\sigma_\alpha\sigma_{\alpha'}\sigma_\alpha = \sigma_{\alpha'}(2\delta_{\alpha,\alpha'} - 1)$ . Notable cases are  $\pi$ -rotations around one of the coordinate axes, e.g.,  $P_{(0,0,\pi)} \equiv [\pi]_z$ . With this notation,  $\theta$ -rotations around the quantization ( $z$ ) axis induce the transformations

$$P_{(0,0,\theta_z)} = [\theta]_z : \sigma_\pm \mapsto e^{\mp i\theta}\sigma_\pm, \quad \sigma_0 \mapsto \sigma_0.$$

Importantly, starting from free evolution ( $y_{j,j'}(t) = \delta_{j,j'}$ ),  $\pi/2$ -pulses allow the generation of purely imaginary-valued switching functions, whilst arbitrary  $\theta$  values typically generate complex-valued switching functions.

Under the above rules, the toggling frame transformation of Eq. (4) induces particular structures in the switching functions. Specifically, one may verify that:

(i) In the Cartesian basis,  $\pi$ -pulses along any coordinate axis  $\alpha$ , corresponding to  $[\pi]_\alpha$ , induce digital switching functions  $y_{\alpha,\alpha'}(t)$  that take values only in  $\{+1, -1\}$  and are “diagonal”, in the sense that  $y_{\alpha,\alpha'}(t) \propto \delta_{\alpha,\alpha'}$ . In contrast, non- $\pi$  pulses generally induce “non-diagonal” switching functions, which can take a continuum of values in  $[-1, 1]$ .

(ii) In the spherical basis, both  $\pi$  and non- $\pi$  pulses induce non-diagonal switching functions  $y_{j,j'}(t)$ . **For instance**, under a rotation of  $\theta$  about  $x$ , the spherical basis transforms as

$$\begin{aligned} [\theta]_x : \sigma_+ &\mapsto \sin^2 \frac{\theta}{2} \sigma_- + i \frac{\sin \theta}{\sqrt{2}} \sigma_0 + \cos^2 \frac{\theta}{2} \sigma_+, \\ \sigma_0 &\mapsto -i \frac{\sin \theta}{\sqrt{2}} \sigma_- + \cos \theta \sigma_0 + i \frac{\sin \theta}{\sqrt{2}} \sigma_+, \\ \sigma_- &\mapsto \cos^2 \frac{\theta}{2} \sigma_- - i \frac{\sin \theta}{\sqrt{2}} \sigma_0 + \sin^2 \frac{\theta}{2} \sigma_+. \end{aligned}$$

Taking  $\theta = \pi$  generates non-zero, non-diagonal switching functions  $y_{\pm 1, \mp 1}(t)$ . Under more general  $\theta$ , both the diagonal and non-diagonal switching functions can take on complex values. This will be very important for our filter design stage, as we will see later (Sec. IV).

Our protocols use sequences composed of qubit rotations, which take the general form given in Eq. (5). In particular,

we consider  $p$  rotations applied at times  $\{t_0, \dots, t_{p-1}\}$  over a total duration  $T$ . The interaction-picture unitary propagator associated to such a control sequence then takes the form

$$\begin{aligned} U_I(T) &= \left[ P_{\vec{\theta}_{p-1}} U_0(t_{p-2}, t_{p-1}) \cdots P_{\vec{\theta}_1} U_0(t_0, t_1) \right] P_{\vec{\theta}_0} \\ &\equiv \left[ \prod_{i=p-1, \dots, 1} P_{\vec{\theta}_i} U_0(t_{i-1}, t_i) \right] P_{\vec{\theta}_0} \\ &= U_{\text{ctrl}}(T) U(T) = \left[ P_{\vec{\theta}_{p-1}} \cdots P_{\vec{\theta}_1} P_{\vec{\theta}_0} \right] U(T). \end{aligned} \quad (6)$$

Here, we have taken  $t_0 \equiv 0$  and time is understood to increase from right to left. In Eq. (6), the propagator  $U_0(t, t')$  denotes free evolution of the system and bath from  $t \mapsto t'$  (i.e.,  $H_{\text{ctrl}}(t) \equiv 0$  in Eq. (3)) and, in Eq. (7), we have expressed the controlled evolution in terms of the toggling-frame propagator,  $U(t) \equiv \mathcal{T} e^{-i \int_0^t ds H(s)}$ , with  $H(t)$  given in Eq. (4).

### C. Reduced qubit dynamics

Evolution under the natural system Hamiltonian and the control in the presence of the environment induces non-trivial dissipative dynamics on the probe qubit, which is captured by the expectation value of relevant physical observables. Let  $O$  denote an invertible qubit observable. Assuming that the system and the bath are initially in a factorized state,  $\rho_{SB}(0) \equiv \rho_0 = \rho_S \otimes \rho_B$ , the time-dependent expectation value in the toggling frame is determined by

$$E(O(t))_{\rho_0} = \langle \text{tr}[U(t)(\rho_S \otimes \rho_B)U(t)^\dagger O] \rangle_c, \quad (8)$$

where  $\langle \cdot \rangle_c$  represents an average over realizations of the classical stochastic process  $\zeta_b(t)$  and, formally, we let  $\rho_B = I_B$  in Eq. (8) if noise is purely classical. By also denoting  $\langle \cdot \rangle_q \equiv \text{tr}_B[\cdot \rho_B]$  and following [41], one can rewrite the above expectation value via a cumulant expansion as

$$\begin{aligned} E(O(t))_{\rho_0} &= \langle \text{tr}_S[\langle O^{-1}U(t)^\dagger O U(t) \rangle_q \rho_S O] \rangle_c \\ &\equiv \text{tr}_S \left[ e^{\sum_{k=1}^{\infty} (-i)^k \frac{\mathcal{C}_O^{(k)}}{k!}} \rho_S O \right] \end{aligned} \quad (9)$$

$$= \text{tr}_S \left[ \langle O^{-1}U(t)^\dagger O U(t) \rangle \rho_S O \right], \quad (10)$$

where in Eq. (10) we have introduced the compact notation  $\langle \cdot \rangle \equiv \langle \langle \cdot \rangle_c \rangle_q$  to denote taking both averages.

The  $k$ -th generalized cumulant  $\mathcal{C}^{(k)}$  entering Eq. (9) is a qubit operator and may be obtained as follows. Realizing that one can rewrite  $O^{-1}U(t)^\dagger O U(t) = \mathcal{T} e^{-i \int_{-T}^T \tilde{H}_O(s) ds}$  with the operator-dependent effective Hamiltonian

$$\tilde{H}_O(t) = \begin{cases} -O^{-1}H(T-t)O & t \in [0, T], \\ H(T+t) & t \in [-T, 0], \end{cases} \quad (11)$$

the cumulant expressions can be obtained from the moment-cumulant generating equation

$$\langle \mathcal{T} e^{-i \int_{-T}^T \tilde{H}_O(s) ds} \rangle = e^{\sum_{k=1}^{\infty} (-i)^k \frac{\mathcal{C}_O^{(k)}}{k!}} = \sum_{k=1}^{\infty} \frac{\mathcal{D}_O^{(k)}}{k!}, \quad (12)$$

where the terms in the Dyson-like expansion in the right hand-side are given by

$$\mathcal{D}_O^{(k)} = k! (-i)^k \int_{-T}^T d_{>}\vec{t}_{[k]} \langle \tilde{H}_O(t_1) \cdots \tilde{H}_O(t_k) \rangle, \quad (13)$$

with  $\int_s^{s'} d_{>}\vec{t}_{[k]} \equiv \int_s^{s'} dt_1 \cdots \int_s^{t_{k-1}} dt_k$ , and the inclusion of factorial term being dictated by convenience. In general, the expansion in Eq. (9) involves an infinite number of terms, and can be exactly truncated only in special scenarios. For example, exact truncation to the second order is possible when the noise model is dephasing-only and Gaussian [41]. Throughout this work, we will not invoke Gaussian noise statistics, but we shall demand that suitable conditions are obeyed to justify truncating the expansion at order two [47].

Under the above assumption, we thus focus only on the first two cumulants. After an appropriate change of variables, allowing us to change the integration domain from  $[-T, T]$  to  $[0, T]$ , and recalling the definition of  $\tilde{H}_O(t)$  in Eq. (11), the first two cumulants can be written as follows:

$$\mathcal{C}_O^{(1)} = \int_0^T dt_1 \left[ C^{(1)}(H(t_1)) - C^{(1)}(\overline{H}_O(t_1)) \right], \quad (14)$$

$$\begin{aligned} \frac{\mathcal{C}_O^{(2)}}{2!} &= \int_0^T d_{>}\vec{t}_{[2]} \left[ C^{(2)}(H(t_1), H(t_2)) \right. \\ &\quad + C^{(2)}(\overline{H}_O(t_2), \overline{H}_O(t_1)) \\ &\quad \left. - C^{(2)}(\overline{H}_O(t_1), H(t_2)) - C^{(2)}(\overline{H}_O(t_2), H(t_1)) \right], \end{aligned} \quad (15)$$

in terms of the toggling frame Hamiltonian  $H(t)$  and its observable-conjugated version  $\overline{H}_O(t) \equiv O^{-1}H(t)O$ , via the cumulant expressions

$$\begin{aligned} C^{(1)}(A) &= \langle A \rangle, \\ C^{(2)}(A, B) &= \langle AB \rangle - \frac{1}{2} \left( \langle A \rangle \langle B \rangle + \langle B \rangle \langle A \rangle \right). \end{aligned}$$

Notice that the average  $\langle \cdot \rangle$  is non-commuting, in the sense that when  $A$  and  $B$  are operators on  $\mathcal{H}_S \otimes \mathcal{H}_B$ , one generally has  $[\langle A \rangle, \langle B \rangle] \neq 0$  and care must be taken during calculations.

We remark that, while evaluating qubit time-evolved observables in the toggling frame is mathematically convenient, in experiments these expectations cannot be measured directly. Nevertheless, they can be related to measurable quantities in either the lab frame or the interaction frame (or, under resonance conditions, a frame which is also co-rotating with the carrier frequency of the control) by additionally implementing an appropriate compensating transformation, leveraging the fact that both the internal qubit Hamiltonian and the applied control propagator in Eq. (7) are known. In practice, if sufficiently fast control is available, this amounts to implementing an additional rotation immediately before measurement, which effectively un-does the rotation generated by the ideal control  $U_{\text{ctrl}}(T)$  [48].

### III. TOOLS FOR SPECTRAL ESTIMATION

#### A. Frequency domain representation

Given the way in which the Hamiltonian enters the reduced dynamics (see Eqs. (10) and (15)), one needs to evaluate expressions with the following general structure:

$$\int d_{>}\vec{t}_{[2]} \langle H(t_1) \overline{H}_O(t_2) \rangle = \sum_{a, a', b, b'} (\sigma_{a'} O^{-1} \sigma_{b'} O) [I_2]_{a, a', b, b'},$$

where the integral

$$[I_2]_{a, a', b, b'} \equiv \int d_{>}\vec{t}_{[2]} y_{a, a'}(t_1) y_{b, b'}(t_2) \langle B_a(t_1) B_b(t_2) \rangle$$

is common to all the terms in the aforementioned reduced dynamics equations. By moving to the frequency domain, both the bath correlators  $\langle B_{b_1}(t_1) \cdots B_{b_k}(t_k) \rangle$  and products of the switching functions  $\{y_{a, a'}(t)\}$  will then enter the dynamics via their corresponding Fourier transform.

Specifically, the influence of bath correlations on the qubit dynamics is captured by the multi-time Fourier transform

$$\langle B_{b_1}(\omega_1) \cdots B_{b_k}(\omega_k) \rangle = \int_{-\infty}^{\infty} d\vec{t} e^{i\vec{\omega} \cdot \vec{t}} \langle B_{b_1}(t_1) \cdots B_{b_k}(t_k) \rangle.$$

We will assume that the noise has zero-mean and is *stationary* which, since we are truncating the cumulant expansion at  $k = 2$ , is captured by the relations

$$\begin{aligned} \langle B_b(\omega) \rangle &= 0, \\ \langle B_{b_1}(\omega) B_{b_2}(\omega') \rangle &= \delta(\omega + \omega') S_{b_1, b_2}(\omega), \end{aligned}$$

where as usual the relevant PSD is defined as

$$S_{b_1, b_2}(\omega) = \int_{-\infty}^{\infty} d\tau e^{-i\omega\tau} \langle B_{b_1}(\tau) B_{b_2}(0) \rangle.$$

The PSD can be naturally separated into two components,  $S_{b_1, b_2}(\omega) = [S_{b_1, b_2}^-(\omega) + S_{b_1, b_2}^+(\omega)]/2$ , depending on the commutator and anticommutator of the noise operators,

$$\begin{aligned} S_{b_1, b_2}^-(\omega) &\equiv \int_{-\infty}^{\infty} d\tau e^{-i\omega\tau} \langle [B_{b_1}(\tau), B_{b_2}(0)] \rangle, \\ S_{b_1, b_2}^+(\omega) &\equiv \int_{-\infty}^{\infty} d\tau e^{-i\omega\tau} \langle \{B_{b_1}(\tau), B_{b_2}(0)\} \rangle. \end{aligned}$$

The ‘‘classical’’ spectrum  $S_{b_1, b_2}^+(\omega)$  is present for both quantum and classical noise, while the ‘‘quantum’’ spectrum  $S_{b_1, b_2}^-(\omega)$  vanishes when the noise is purely classical and, hence, commuting. We draw a further distinction between spectra whose indices refer to the same noise operator, the ‘‘self’’- spectra  $S_{b_1, b_2}^{\pm}(\omega)|_{b_2=b_1}$ , or different noise operators, the ‘‘cross’’- spectra  $S_{b_1, b_2}^{\pm}(\omega)|_{b_2 \neq b_1}$  [13, 41]. The relations between the various spectra depend on the coordinate system:

(i) Since  $B_{\alpha}(t)^{\dagger} = B_{\alpha}(t)$  in Cartesian coordinates,  $i[B_{\alpha_1}(t), B_{\alpha_2}(t')]$  and  $\{B_{\alpha_1}(t), B_{\alpha_2}(t')\}$  are self-adjoint, which in turn implies that

$$[S_{\alpha_1, \alpha_2}^{\pm}(\omega)]^* = S_{\alpha_2, \alpha_1}^{\pm}(\omega) = \pm S_{\alpha_1, \alpha_2}^{\pm}(-\omega). \quad (16)$$

(ii) In spherical coordinates, as noted, bath operators corresponding to  $j = \pm 1$  are not self-adjoint. In this case,  $B_j(t)^\dagger = B_{-j}(t)$  and it follows that

$$[S_{j,l}^\pm(\omega)]^* = S_{-l,-j}^\pm(\omega) = \pm S_{-j,-l}^\pm(-\omega). \quad (17)$$

For a more physical interpretation of the quantum and classical spectra, note that under free evolution for  $\alpha \in \{x, y\}$ , the rates of bath-induced absorption and emission are determined by the self-spectra  $S_{\alpha,\alpha}(\Omega)$  and  $S_{\alpha,\alpha}(-\Omega)$ , respectively [49]. If the noise is classical and  $S_{\alpha,\alpha}^-(\omega) \equiv 0$ , then  $S_{\alpha,\alpha}(\omega) = S_{\alpha,\alpha}^+(\omega)/2$ , which is an even function of  $\omega$ . Consequently,  $S_{\alpha,\alpha}(\Omega) = S_{\alpha,\alpha}(-\Omega)$  and the rates of absorption and emission are always equal. In contrast, for quantum noise with  $S_{\alpha,\alpha}^-(\omega) \neq 0$ , the rates are not equal in general. In the spherical basis, as we shall soon see, the rates of absorption and emission are determined by the cross-spectra  $S_{+1,-1}(\Omega)$  and  $S_{-1,+1}(-\Omega)$ , respectively. Thus, nonzero  $S_{+1,-1}^-(\omega)$  and  $S_{-1,+1}^-(\omega)$  indicate potentially unequal absorption and emission rates, a signature of quantum noise.

Similar to the description of bath-induced noise in terms of spectra, the effect of the control may be compactly described in the frequency domain by first and second order *fundamental FFs* [43], namely,

$$\begin{aligned} F_{a,a'}^{(1)}(\omega, T) &= \int_0^T dt y_{a,a'}(t) e^{i\omega t}, \\ F_{a,a';b,b'}^{(2)}(\omega, \omega', T) &= \int_0^T dt \int_0^t dt' y_{a,a'}(t) y_{b,b'}(t') e^{i(\omega t + \omega' t')}. \end{aligned} \quad (18)$$

The above fundamental FFs enter the reduced dynamics of the qubit in the combinations [41, 50]:

$$\begin{aligned} G_{a,a';b,b'}^-(\omega, \omega', T) &= F_{a,a';b,b'}^{(2)}(\omega, \omega', T) \\ &\quad - F_{b,b';a,a'}^{(2)}(\omega', \omega, T), \end{aligned} \quad (19)$$

$$\begin{aligned} G_{a,a';b,b'}^+(\omega, \omega', T) &= F_{a,a';b,b'}^{(2)}(\omega, \omega', T) \\ &\quad + F_{b,b';a,a'}^{(2)}(\omega', \omega, T) \\ &= F_{a,a'}^{(1)}(\omega, T) F_{b,b'}^{(1)}(\omega', T). \end{aligned} \quad (20)$$

Combining our observations in the frequency domain representation, we can determine explicit expressions for the cumulants in Eqs. (14)-(15). First, recalling that the noise is zero mean, one has that  $\mathcal{C}_O^{(1)} = 0$  in both coordinate representations, for arbitrary  $O$ . While general closed-form expressions may be obtained for the second cumulant, we specialize to the simpler and practically relevant case of Pauli observables. In the spherical representation, direct calculation yields

$$\begin{aligned} \frac{\mathcal{C}_{\sigma_\gamma}^{(2)}}{2} &= \sum_{l,l',j,j'} \int_{-\infty}^{\infty} \frac{d\omega}{2\pi} F_{j,j';l,l'}^{(2)}(\omega + j\Omega, -\omega + l\Omega, T) \times \\ &\quad \left[ (\sigma_{j'} \sigma_{l'} - \sigma_\gamma \sigma_{j'} \sigma_\gamma \sigma_{l'}) S_{-j,-l}(-\omega) \right. \\ &\quad \left. + (\sigma_\gamma \sigma_{l'} \sigma_{j'} \sigma_\gamma - \sigma_\gamma \sigma_{l'} \sigma_\gamma \sigma_{j'}) S_{-l,-j}(\omega) \right], \end{aligned} \quad (21)$$

where the  $\Omega$ -displacement in the frequency arguments of the fundamental FFs arises due to the  $e^{i\Omega t}$  factors in the spherical Hamiltonian [Eq. (4)]. This expression, combined with Eq. (9) for  $O = \sigma_z$ , enables us to shed more light on the role of the spherical spectra in the qubit dynamics. Neglecting correlations between the transverse and longitudinal noise operators, to first order in  $T$  under free evolution,

$$\begin{aligned} E[\sigma_z(T)]_{|+z\rangle\langle+z| \otimes \rho_B} &\approx 1 - 2TS_{-1,+1}(-\Omega), \\ E[\sigma_z(T)]_{|-z\rangle\langle-z| \otimes \rho_B} &\approx -1 + 2TS_{+1,-1}(\Omega), \end{aligned}$$

where  $\sigma_z|\pm z\rangle = \pm|\pm z\rangle$ . Thus,  $S_{-1,+1}(-\Omega)$  sets the rate of bath-induced emission from  $|+z\rangle$  to  $|-z\rangle$ , while  $S_{+1,-1}(\Omega)$  sets the rate of bath-induced absorption from  $|-z\rangle$  to  $|+z\rangle$ .

In Cartesian coordinates, the second cumulant is given by

$$\begin{aligned} \frac{\mathcal{C}_{\sigma_\gamma}^{(2)}}{2} &= \sum_{\alpha,\beta,\alpha',\beta'} \sigma_\alpha \sigma_\beta \int_{-\infty}^{\infty} \frac{d\omega}{4\pi} S_{\alpha',\beta'}^{f_\alpha^\gamma f_\beta^\gamma f_\beta^\alpha}(\omega) \times \\ &\quad \left[ G_{\alpha,\alpha';\beta,\beta'}^{f_\alpha^\gamma f_\beta^\gamma}(\omega, -\omega, T) + f_\alpha^\gamma G_{\alpha,\alpha';\beta,\beta'}^+(\omega, -\omega, T) \right], \end{aligned} \quad (22)$$

with  $f_\alpha^\gamma = \text{tr}[\sigma_\alpha \sigma_\gamma \sigma_\alpha \sigma_\gamma]/2$ , which is hauntingly similar to the expression derived in [41] for a multiqubit dephasing model, i.e., when all operators are mutually commuting (see in particular Eq. (27) therein). The only seemingly minor difference is the  $f_\beta^\alpha$  superscript in  $S_{\alpha',\beta'}^{f_\alpha^\gamma f_\beta^\gamma f_\beta^\alpha}(\omega)$  which, however, will have significant consequences in terms of the symmetries needed to extract all the noise spectra (see Sec. IV).

Again, we stress that here we are truncating the expansion to the second order based on a suitable convergence argument (for instance, weak coupling) and not because we are —em a priori invoking a Gaussian property of the noise. In fact, notice that even when the Gaussian assumption is in place, the non-commuting, multi-axis nature of the noise prevents the cumulant series from truncating exactly, unlike for single-axis noise [6, 41].

## B. QNS via frequency comb

The interplay between FFs and power spectra is the key element in the QNS protocols we consider. The aim of these protocols is to estimate the full set of dynamically relevant spectra  $\{S_{b_1, b_2}^\pm(\omega)\}$  by studying the response of the probe system to the control while in the presence of the target noise. Mathematically, this entails two key steps: first, isolating the integrals that involve a spectrum of interest by choosing an appropriate set of observables and initial states; next, deconvolving each such integral to obtain an appropriate estimate.

The first problem can be addressed by preparing eigenstates of the Pauli basis  $\sigma_\alpha$ , for  $\alpha = x, y, z$ , measuring in the Pauli basis, and combining the resulting expectation values into experimentally accessible quantities. The preparation and measurement procedure simplifies if the system has known symmetries, as one may appreciate by considering a purely dephasing classical noise model, i.e., one for which  $B_a(t) \propto \zeta_a(t) \delta_{a,z} I_B$ . Using control that preserves the dephasing character of the Hamiltonian, e.g.,  $[\pi]_x$  pulses,

the expectation value of  $\sigma_x$  when the qubit is initialized in  $(I_S + \sigma_x)/2 = |+\rangle\langle +|$  is given by

$$\begin{aligned} \log[E(\sigma_x(t))_{|+\rangle\langle +| \otimes \rho_B}] &= \log[\text{tr}(e^{-\mathcal{C}^{(2)}/2!} |+\rangle\langle +| \sigma_x)] \\ &= -\frac{1}{\pi} \int_{-\infty}^{\infty} d\omega G_{z,z;z,z}^+(\omega, -\omega, T) S_{z,z}^+(\omega). \end{aligned}$$

A single preparation and measurement setting is enough to isolate the integral containing the relevant noise information.

The second issue, namely, extracting the noise information once the integral has been isolated, has been the object of many recent studies [2, 3, 5, 6, 40, 41, 48]; in particular, DD QNS based on a frequency-comb approach has been widely employed [19]. The basic idea behind such an approach is to ensure that each of the integrals that can be isolated can be further *discretized and truncated* in a systematic way, by use of control. The objective is to guarantee that any of the aforementioned integrals takes the form

$$I = \int_{-\infty}^{\infty} d\omega G(\omega) S(\omega) \simeq A \sum_{k=0}^K G(k\omega_0) S(k\omega_0), \quad (23)$$

where both the fundamental frequency  $\omega_0$  and the proportionality constant  $A$  are determined by the choice of control, and the highest harmonic  $K$  is adjusted so that  $S(\omega)$  is reasonably small for  $\omega \geq K\omega_0$  (see, however, further discussion in Sec. VI). If this can be achieved, then each integral is basically a linear equation involving the unknown quantities,  $S(k\omega_0)$ , along with known, tunable, control-dependent coefficients  $AG(k\omega_0)$ . Since a given experiment provides access to the value of  $I$ , it is then possible to generate a system of linear equations by changing the control being used, from which an estimate of the target power spectra can ultimately be inferred.

The discretization described above may be achieved by a suitable choice of control. To make contact with existing tools, it is useful to note that, given the form of the dynamical equations, there are two kinds of FFs we have to be concerned with, namely,  $G_{a,a';b,b'}^+(\omega, \omega', T)$  and  $G_{a,a';b,b'}^-(\omega, \omega', T)$  – formally very similar to the setting of multiqubit pure dephasing we analyzed in [41, 50]. As shown there, the key to generating a frequency comb is the ability to design switching functions exhibiting one or more of the following symmetries:

- (i)  $T_c$  periodicity, i.e.,  $y_{a,a'}(t) = y_{a,a'}(t + T_c)$ , for  $T_c > 0$ .
- (ii) Displacement (anti-)symmetry at time scale  $[0, \tau]$ , i.e., for  $t \in [0, \tau/2]$ ,  $y_{a,a'}(t) = \pm y_{a,a'}(t + \tau/2)$ .
- (iii) Mirror (anti-)symmetry at time scale  $[0, \tau]$ , i.e., for  $t \in [0, \tau/2]$ ,  $y_{a,a'}(\tau/2 - t) = \pm y_{a,a'}(t + \tau/2)$ .

Most relevant to this paper, one can show [3, 50] that if a control sequence of duration  $T_c$  is repeated  $M \gg 1$  times over a total duration  $T = MT_c$ , a frequency comb is created in which an arbitrary first-order FF is directly expressible in terms of its single-cycle counterpart. For FFs of the  $G^+$ -type,

the frequency comb takes the form

$$\begin{aligned} G_{a,a';b,b'}^+(\omega, -\omega, MT_c) &= \frac{\sin^2(M\frac{\omega T_c}{2})}{\sin^2(\frac{\omega T_c}{2})} G_{a,a';b,b'}^+(\omega, -\omega, T_c) \\ &\simeq \frac{2\pi M}{T_c} \sum_k \delta(\omega - k\omega_0) G_{a,a';b,b'}^+(\omega, -\omega, T_c), \end{aligned} \quad (24)$$

where  $\omega_0 = 2\pi/T_c$ . For the  $G^-$ -type FFs, in addition to control repetition ( $T_c$ -periodicity), one of the switching functions entering the FF in Eqs. (18) and (20) must be displacement anti-symmetric and the other symmetric. This symmetry condition combined with repetition generates another comb,

$$\begin{aligned} G_{a,a';b,b'}^-(\omega, -\omega, MT_c) \\ \simeq \frac{2\pi}{T_c} \sum_k (-1)^k \delta(\omega - k\omega_0) G_{a,a';b,b'}^+(\omega, -\omega, T_c/2). \end{aligned}$$

Additionally, mirror symmetry in the interval  $[0, T_c]$  (or,  $[0, T_c/2]$ ) can be leveraged to control the real or imaginary character of the filters  $G_{a,a';b,b'}^+(\omega, -\omega, T_c)$  (or,  $G_{a,a';b,b'}^+(\omega, -\omega, T_c/2)$ , respectively).

By combining the tools described above, we showed how all the spectra relevant to a multiqubit dephasing Gaussian noise model could be reconstructed [41]. A caveat of having to deal with both types of filters is their **different scaling with the number of repetitions,  $M$** . While one can, in principle, work around this by a careful choice of controls [41], this imposes constraints on the types of sequences that can be used, which in turn leads to complications in reconstructing spectra that are filtered by the  $G^-$ -type FFs. In contrast to single-qubit dephasing, the complexity of the multiqubit dephasing protocol arises from the fact that the system operators in  $H(t)$  are spanned by a richer, albeit still commuting, algebra. In the single-qubit multi-axis setting, the situation is seemingly more complex, as the system part of the Hamiltonian is additionally spanned by an algebra which is *non-commuting*. Following this reasoning, one would expect that, at the very least, all of the same symmetries should be necessary in our current scenario. Surprisingly, as we will see in Sec. IV B, the structure of Eq. (22) implies that *only  $G^+$  filters* are relevant for our purposes. This, in turn, **affords the use of a smaller set of symmetries (just repetition and mirror)** and, as an added benefit, the  $M$ -scaling complication we highlighted is absent.

### C. Frame-tilting control sequences

While repetition of base sequences exhibiting the aforementioned symmetries is essential to generate the comb, the choice of pulse types in the base sequences is crucial to access all of the spectra, whenever multiple kinds of spectra simultaneously influence the dynamics. In [41], an important design principle was the use of “non-diagonal” control sequences, capable of generating non-trivial switching functions  $y_{a,b}(t)$  not proportional to  $\delta_{a,b}$ .

Here, we further introduce more general “frame-tilting” control sequences, which contain the aforementioned approach as a special case and are closely related to “twisted

decouplers” [45]. Just before the application of pulse  $i + 1$  at time  $t_i$ , recall from Eq. (7) that the control propagator is given by  $U_{\text{ctrl}}(t_i) = P_{\tilde{\theta}_{i-1}} \cdots P_{\tilde{\theta}_0}$ . In a tilted DD sequence, the trick is to choose the pulses  $P_{\tilde{\theta}_{i-1}}, \dots, P_{\tilde{\theta}_0}$ , so that at each  $t_i$ , the control propagator can be written in terms of a fixed ( $i$ -independent) “tilting pulse”  $P_{\text{tilt}}$  and a desired “target pulse”  $P_{\tilde{\theta}_i}$ , namely,

$$U_{\text{ctrl}}(t_i) = P_{\tilde{\theta}_{i-1}} \cdots P_{\tilde{\theta}_0} = P_{\text{tilt}} P_{\tilde{\theta}_i}. \quad (25)$$

At each time  $t_i$ , the control propagator then induces the toggling frame transformation

$$\sigma_a \mapsto U_{\text{ctrl}}^\dagger(t_i) \sigma_a U_{\text{ctrl}}(t_i) = P_{\tilde{\theta}_i}^\dagger \left[ P_{\text{tilt}}^\dagger \sigma_a P_{\text{tilt}} \right] P_{\tilde{\theta}_i}, \quad \forall a.$$

In this way, we can “tilt” the operator basis  $\{\sigma_a\}$  at every interval, and still have enough freedom in  $P_{\tilde{\theta}_i}$  to generate a non-trivial switching function after the frame transformation. Similar to non-diagonal base sequences in [41], this effectively grants us the ability to control which bath operator couples to which system operator.

Of particular relevance in the subsequent discussion will be the tilting transformation defined by  $P_{\text{tilt}} = [\frac{\pi}{4}]_x$ . Under this transformation one finds that

$$\begin{aligned} \left[ \frac{\pi}{4} \right]_x : \sigma_+ &\mapsto \sin^2 \frac{\pi}{8} \sigma_- + i \frac{\sigma_0}{2} + \cos^2 \frac{\pi}{8} \sigma_+, \\ \sigma_0 &\mapsto \frac{1}{2} \left( -i \sigma_- + \sqrt{2} \sigma_0 + i \sigma_+ \right), \\ \sigma_- &\mapsto \cos^2 \frac{\pi}{8} \sigma_- - i \frac{\sigma_0}{2} + \sin^2 \frac{\pi}{8} \sigma_+, \end{aligned} \quad (26)$$

which in turn implies that in a given time interval where the transformation has been executed, all the switching functions  $y_{j,j'}(t)$  are in general non-vanishing, i.e., they are non-diagonal as desired. While other tilting transformations are of course possible, the above is particularly convenient when the qubit quantization axis is along  $\sigma_z$ , as we will see in Sec. V.

## IV. PROTOCOLS FOR COMB-BASED MULTIAXIS QNS

### A. Accessible quantities

The first step towards constructing an explicit QNS protocol is understanding what information is accessible to the experimentalist when the ability to prepare different initial states and measure in different bases is exploited and, in particular, which of the various integrals appearing in  $\mathcal{C}_O^{(2)}$  can be isolated. For concreteness, we shall assume the ability to prepare any eigenstate of the Pauli basis, and measure in any direction. In other words, with  $\rho_S \in \{\eta_{\pm, \alpha} = (I_S \pm \sigma_\alpha)/2\}$ , we assume we have access to all the expectation values

$$E(\sigma_\gamma(T))_{\eta_{\pm, \alpha} \otimes \rho_B} = \text{tr} \left[ e^{\mathcal{C}_\gamma} \frac{\sigma_\gamma \pm \sigma_\alpha \sigma_\gamma}{2} \right],$$

where we have introduced the observable-dependent qubit operator  $\mathcal{C}_\gamma \equiv \sum_k (-i)^k \mathcal{C}_{\sigma_\gamma}^{(k)}/k!$  and  $\alpha, \gamma \in \{x, y, z\}$ . We de-

note the decomposition of  $\mathcal{C}_\gamma$  in the Pauli basis by

$$\mathcal{C}_\gamma \equiv \sum_{\beta=0,x,y,z} \mathcal{C}_{\gamma, \beta} \sigma_\beta. \quad (27)$$

By combining expectation values of  $\sigma_\gamma$  for different initial states of the qubit, it is then possible to isolate each of the  $\mathcal{C}_{\gamma, \beta}$  terms individually. Consider the the experimentally accessible quantities defined by the linear combinations

$$\mathcal{M}_{r, \alpha}^{(x)} \equiv E(\sigma_x(T))_{\eta_{+1, x} \otimes \rho_B} + r E(\sigma_x(T))_{\eta_{-1, x} \otimes \rho_B}.$$

If  $\sigma_\gamma = \sigma_x$  and  $r = \pm 1$ , for example, these can be written as functions of the  $\mathcal{C}_{x, \beta}$  as follows:

$$\mathcal{M}_{+, x}^{(x)} = \frac{2e^{C_{x,0}} C_{x,x} \sinh |C_x|}{|C_x|}, \quad (28)$$

$$\mathcal{M}_{-, x}^{(x)} = 2e^{C_{x,0}} \cosh |C_x|, \quad (29)$$

$$\mathcal{M}_{-, y}^{(x)} = \frac{2ie^{C_{x,0}} C_{x,z} \sinh |C_x|}{|C_x|}, \quad (30)$$

$$\mathcal{M}_{-, z}^{(x)} = -\frac{2ie^{C_{x,0}} C_{x,y} \sinh |C_x|}{|C_x|}, \quad (31)$$

where  $|C_x| \equiv \sqrt{C_{x,x}^2 + C_{x,y}^2 + C_{x,z}^2}$ . From these expressions, the quantities  $\mathcal{C}_{x, \beta}$  can be obtained by judiciously applying trigonometric identities. Similar methods allow us to obtain the coefficients  $\mathcal{C}_{\gamma, \beta}$  for other observables. Recalling that we are truncating the cumulant expansion to second order, it follows from Eq. (27) that we then have access to all the quantities  $\mathcal{C}_{\gamma, \beta} \simeq \text{tr}[\mathcal{C}_{\sigma_\gamma}^{(2)} \sigma_\beta]/2$ .

### B. Balanced and imbalanced filters

Given the access to the projections of  $\mathcal{C}_{\sigma_\gamma}^{(2)}$  on each axis and Eqs. (21)-(22), one recognizes that the filters present in the problem can be separated into two classes according to the frequency displacement induced by  $H_S$ . The filters

$$G_{a, a'; b, b'}^\pm(\omega + s\Omega, -\omega + s'\Omega, T), \quad s, s' \in \{-1, 0, +1\},$$

are said to be *balanced* when  $(s + s')\Omega = 0$  and *imbalanced* when  $(s + s')\Omega \neq 0$ . This distinction proves crucial. Because  $\omega + s\Omega = -(-\omega + s'\Omega)$  for a balanced displacement, taking  $\omega' \equiv \omega + s\Omega$  produces filters of the form  $G_{a, a'; b, b'}^\pm(\omega', -\omega', T)$ . For such filters, the discussion in Sec. III B suggests that one just needs to generate the necessary symmetries to produce a comb. In other words, if these were the only FFs entering the problem, then the results obtained for dephasing models in [41] would, in principle, seamlessly extend to the general decoherence scenario. However, for imbalanced filters, which do not have the simple form  $G_{a, a'; b, b'}^\pm(\omega', -\omega', T)$ , a comb *cannot* be generated by simply applying the aforementioned symmetries and a different treatment is needed.

### 1. QNS and balanced filters

As highlighted earlier, reconstructing the power spectra via a balanced filter requires the use of the aforementioned set of well-established symmetries and indeed, at a first glance, it would seem that it is necessary to be able to impose any of them. However, as it turns out, the fact that we are working with a single-qubit probe reduces the need for some of them.

The simplest scenario arises when  $\Omega = 0$ , as in this case only  $G_{a,a';b,b'}^\pm(\omega, -\omega, T)$  filters appear in the dynamics. Furthermore, a close analysis of Eq. (22), shows that it is possible to combine observables in such way that *all* spectra are filtered by  $G_{a,a';b,b'}^+(\omega, -\omega, T)$  filters. This is a striking difference between the two-qubit single-axis and the single-qubit multi-axis scenarios, which can be traced back to the seemingly innocuous  $f_{\alpha'}^\alpha$  superscript in Eq. (22). For example, one can reconstruct  $\text{Re}[S_{x,z}^\pm(\omega)]$  and  $\text{Im}[S_{x,z}^\pm(\omega)]$  from the relations

$$\begin{aligned} C_{x,y} - C_{z,y} &= 4i \int_0^\infty \frac{d\omega}{2\pi} \left( \text{Im}[S_{x,z}^+(\omega)] \text{Im}[G_{x,x,z,z}^+(\omega, T)] \right. \\ &\quad \left. - \text{Re}[S_{x,z}^+(\omega)] \text{Re}[G_{x,x,z,z}^+(\omega, T)] \right), \\ C_{y,y} &= 4 \int_0^\infty \frac{d\omega}{2\pi} \left( \text{Re}[S_{x,z}^-(\omega)] \text{Im}[G_{x,x,z,z}^+(\omega, T)] \right. \\ &\quad \left. + \text{Im}[S_{x,z}^-(\omega)] \text{Re}[G_{x,x,z,z}^+(\omega, T)] \right), \end{aligned}$$

simply by using repetition symmetry. The remaining spectra can be obtained in a similar fashion by combining  $C_{\alpha,\beta}$ 's and using frame-tilting base sequences, i.e., both diagonal and non-diagonal control. We stress that this does not mean that  $G^-$  filters do not enter the dynamics of the qubit (see Appendix A); they just are not necessary for QNS purposes.

The general  $\Omega \neq 0$  scenario shares some similar features. In particular, a detailed analysis of Eq. (21) shows that, while both balanced and imbalanced filters are now present, one may still combine  $C_{\alpha,\beta}$  quantities in a way that only  $G_{a,a';b,b'}^+(\omega + s\Omega, -\omega + s'\Omega, T)$  filters are relevant to the QNS problem (we show this explicitly in the next section). In turn, this implies that, similar to the single-qubit single-axis problem [3, 6], sequence repetition suffices for QNS – provided one can find a compatible mechanism to deal with the imbalanced  $G^+$  filters, to which we turn now.

### 2. QNS and imbalanced filters

Imbalanced filters pose a different challenge. To see this, consider first the effect of repeating a given base sequence  $M$  times. Then, the filters relevant to spectroscopy take the form

$$\begin{aligned} &G_{a,a';b,b'}^+(\omega + s\Omega, -\omega + s'\Omega, MT_c) = \\ &e^{i(s+s')\frac{\Omega T_c}{2}} \frac{\sin^2(M\frac{\omega T_c}{2})}{\sin^2(\frac{\omega T_c}{2})} G_{a,a';b,b'}^+(\omega + s\Omega, -\omega + s'\Omega, T_c). \end{aligned}$$

The displacement in the frequency argument leads to an extra exponential factor that does *not* appear in the expression leading to the comb, Eq. (24). Formally, when  $\Omega \neq 0$ , we

may envision imposing a *synchronization* condition between the qubit energy scale and the periodicity of the applied control to recover the desired comb-generating expression. That is, we may demand that  $\Omega T_c/2 = m\pi$ , for some integer  $m$ , such that the  $e^{i(s+s')\frac{\Omega T_c}{2}} = \pm 1$ . In other words, control repetition along with the synchronization condition are enough to generate a comb in all relevant filters for arbitrary values of  $\Omega$ .

### 3. Imbalanced filters in the large qubit-splitting regime

While, mathematically, synchronization solves the problem, one needs to consider whether it can be realistically achieved. Even with perfect knowledge of  $\Omega$ , let us assume that the precision in timing is  $\delta t$ , that is, we can apply pulses at a times  $t_i \pm \delta t$ . In this situation, guaranteeing the synchronization condition implies then that  $\Omega \delta t/2 \ll \pi$ . In turn, this imposes the constraint  $\delta t \ll 2\pi/\Omega$ , which may be unrealistic when  $\Omega$  is sufficiently large – as is the case in many realistic devices (see also Sec. V).

Fortunately, this potentially problematic regime has a redeeming property: when  $\Omega T$  is sufficiently large, *imbalanced filters become negligible*. Thus, spectra that enter the dynamics only via convolutions with such filters are effectively irrelevant. In essence, this result follows from separating the two important timescales in the problem, namely, the evolution time  $T$  and  $1/\Omega$ , similar in spirit to the secular approximation often used in open quantum systems [51]. A detailed derivation of this argument is provided in Appendix B.

The above implies that, crucially, when  $\Omega T \gg 1$  and the imbalanced filters are negligible, the *only* spectra contributing to the qubit dynamics are  $S_{\pm 1, \mp 1}^\pm(\omega)$  and  $S_{0,0}^\pm(\omega)$ . Thus, these spectra are the only ones that need to be reconstructed in order to model the qubit dynamics. Interestingly, extending the argument presented here to higher order filters would imply that, in the  $\Omega T \gg 1$  regime, the non-unitary effective propagator  $\langle \mathcal{T} e^{-i \int_{-T}^T \tilde{H}_O(s) ds} \rangle$  (see Eqs. (10) and (13)) acting on the qubit can always be written as  $e^{A I_S + B \sigma_z}$ . We highlight that despite this simple single-axis form, Eq. (10) allows for both dephasing and relaxation in the dynamics.

## V. ILLUSTRATIVE RESULTS

We are now ready to showcase the key steps allowing us to perform QNS of a multi-axis noise model in a concrete example. We will focus on the physically relevant regime of large qubit splitting – more specifically,  $\Omega T \gg 1$ . Our aim is three-fold: (i) to show in detail the validity of our previous claims regarding the role of  $G^+$ -filters in multi-axis QNS; (ii) to verify that only a small set of spectra contribute to the dynamics in this parameter regime; and (iii) to provide quantitative numerical results that will also allow us to discuss some of the potential limitations of the comb approach.

Observable	Expectation values	Accessible coefficients
$\sigma_x$	$E(\sigma_x(T))_{\eta_{\pm,\alpha} \otimes \rho_B}$	$C_{x,x}(T), C_{x,0}(T)$
$\sigma_y$	$E(\sigma_y(T))_{\eta_{\pm,\alpha} \otimes \rho_B}$	$C_{y,y}(T), C_{y,0}(T)$
$\sigma_z$	$E(\sigma_z(T))_{\eta_{\pm,\alpha} \otimes \rho_B}$	$C_{z,z}(T), C_{z,0}(T)$

TABLE I. Summary of expectation values necessary for determining the experimentally accessible quantities  $\{Q_p(T)\}$  used in our protocol. For each observable, qubit initialization in a complete set of initial states is assumed,  $\eta_{\pm,\alpha} = (I_S + \sigma_\alpha)/2 = |\pm\alpha\rangle\langle\pm\alpha|$ , with  $\alpha \in \{x, y, z\}$ . The relation between the  $C_{\alpha,\beta}$  and the  $Q_p(T)$  is given in Eq. (32). While in the explicit protocol we present only  $C_{z,\beta}$  and  $C_{x,\beta}$ ,  $C_{y,\beta}$  could be similarly used in place of  $C_{x,\beta}$ .

## A. Protocol implementation

### 1. Physical observables

To start, we explore the structure of the accessible quantities  $C_{\alpha,\beta}$ , that determine the decomposition in Eq. (27). A direct calculation shows that the following four combinations,

$$\begin{aligned} Q_1(T) &= \frac{1}{2}(C_{z,0} + C_{z,z}), & Q_2(T) &= \frac{1}{2}(C_{z,0} - C_{z,z}), \\ Q_3(T) &= C_{x,0}, & Q_4(T) &= C_{x,x}, \end{aligned} \quad (32)$$

are both sufficient and practically convenient to reconstruct all the necessary spectra. That the quantities  $\{Q_p(T)\}$  are experimentally accessible follows by noting that they can be obtained by combining an appropriate set of Pauli expectation values and leveraging Eqs. (28)-(31). While a summary is given in Table I, we further illustrate the procedure by showing the explicit process for obtaining  $C_{x,0}$  and  $C_{x,x}$ . First, note that from our expressions for  $\{\mathcal{M}_{\pm,\alpha}^{(x)}\}$ , one finds that

$$\begin{aligned} C_{x,0} &= \frac{1}{2} \log \left\{ \frac{1}{4} \left[ \left( E(\sigma_x(T))_{\eta_{+,x} \otimes \rho_B} - E(\sigma_x(T))_{\eta_{-,x} \otimes \rho_B} \right)^2 \right. \right. \\ &\quad - \left( E(\sigma_x(T))_{\eta_{+,x} \otimes \rho_B} + E(\sigma_x(T))_{\eta_{-,x} \otimes \rho_B} \right)^2 \\ &\quad + \left( E(\sigma_x(T))_{\eta_{+,y} \otimes \rho_B} - E(\sigma_x(T))_{\eta_{-,y} \otimes \rho_B} \right)^2 \\ &\quad \left. \left. + \left( E(\sigma_x(T))_{\eta_{+,z} \otimes \rho_B} - E(\sigma_x(T))_{\eta_{-,z} \otimes \rho_B} \right)^2 \right] \right\}. \end{aligned}$$

With this one proceeds to extract  $|C_x|$  by inverting Eq. (29). This information is then sufficient to obtain  $C_{x,x}$  from Eq. (28). Indeed, algebraic manipulations yield

$$C_{x,x} = |C_x| e^{-C_{x,0}} \frac{E(\sigma_x(T))_{\eta_{+,x} \otimes \rho_B} + E(\sigma_x(T))_{\eta_{-,x} \otimes \rho_B}}{2 \sinh |C_x|},$$

in terms of parameters that depend solely on the expectations  $\{E(\sigma_x(T))_{\eta_{\pm,\alpha} \otimes \rho_B}\}$ . A similar procedure works for  $\{C_{z,\beta}\}$ .

In principle, the method described above enables us to obtain each  $C_{\alpha,\beta}$  *exactly*, using 6 total expectation values. It is worth noting that, for times sufficiently small to permit a linearization of Eq. (12), producing  $e^{\mathcal{L}\tau} \approx I_S + \sum_{\beta} C_{\gamma,\beta} \sigma_{\beta}$ , the quantities  $Q_p(T)$  can be expressed as linear combinations of

qubit expectation values,

$$Q_1(T) \approx \frac{E(\sigma_z(T))_{\eta_{+,z} \otimes \rho_B} - 1}{2} \quad (33)$$

$$Q_2(T) \approx -\frac{E(\sigma_z(T))_{\eta_{-,z} \otimes \rho_B} + 1}{2} \quad (34)$$

$$Q_3(T) \approx \frac{E(\sigma_x(T))_{\eta_{+,x} \otimes \rho_B} - E(\sigma_x(T))_{\eta_{-,x} \otimes \rho_B}}{2} - 1 \quad (35)$$

$$Q_4(T) \approx \frac{E(\sigma_x(T))_{\eta_{+,x} \otimes \rho_B} + E(\sigma_x(T))_{\eta_{-,x} \otimes \rho_B}}{2}. \quad (36)$$

Although these expressions are not exact, they allow each  $Q_p(T)$  to be obtained using *at most two* expectation values, which may be advantageous in practice.

When the cumulant expansion is truncated at second order and  $C_{\gamma,\beta} \simeq \text{tr}[C_{\sigma_{\gamma}}^{(2)} \sigma_{\beta}]/2$ , the statement regarding sufficiency of the four quantities  $Q_p(T)$  follows from the observation that each can be expressed as

$$Q_p(T) = \sum_{j,l=-1,0,1} \int_{-\infty}^{\infty} \frac{d\omega}{2\pi} \mathcal{G}_{j,l}^{(p)}(\omega, T) S_{j,l}(\omega), \quad (37)$$

where the generalized FFs  $\mathcal{G}_{j,l}^{(\alpha,\beta)}(\omega, T)$  are functions of the  $G^+$  and  $G^-$  filters,

$$\begin{aligned} \mathcal{G}_{-j,-l}^{(1)}(\omega, T) &= G_{j,1;l,-1}^+(\omega + j\Omega, -\omega + l\Omega, T), \\ \mathcal{G}_{-j,-l}^{(2)}(\omega, T) &= G_{j,-1;l,1}^+(\omega + j\Omega, -\omega + l\Omega, T), \\ \mathcal{G}_{-j,-l}^{(3)}(\omega, T) &= 2G_{-j,0;-l,0}^+(\omega + j\Omega, -\omega + l\Omega, T) \\ &\quad - \sum_{j',l'=-1,1} \frac{j'l'}{2} G_{j,j';l,l'}^+(\omega + j\Omega, -\omega + l\Omega, T), \\ \mathcal{G}_{-j,-l}^{(4)}(\omega, T) &= \sum_{\substack{j',l'=-1,0,1 \\ |j'+l'|=1}} (l' - j') G_{j,j';l,l'}^+(\omega + j\Omega, -\omega + l\Omega, T). \end{aligned}$$

The form of these generalized FFs supports our previous claim: since all spectra are represented, only  $G^+$ -type filters are necessary for QNS, and thus sequence repetition suffices to ensure the appearance of the frequency comb. Moreover, since we are concerned with the  $\Omega T \gg 1$  regime, terms involving imbalanced filters can be neglected and the sum in Eq. (37) is effectively restricted by the condition  $j + l = 0$ .

### 2. Filter design principles

Having established that all of the integrals can be deconvolved via a frequency comb by using control repetition, the remaining key aspect of the protocol is that of filter design, i.e., we need to find control sequences whose FFs are capable of sampling the full spectra. This is critically important in the case of quantum noise. Recall from Eqs. (16)-(17) that the quantum components of the spectra,  $S_{j,l}^-(\omega)$ , and the classical components,  $S_{j,l}^+(\omega)$ , are odd and even functions of  $\omega$ , respectively. It then follows from Eq. (37) that  $S_{j,l}^-(\omega)$

can only be reconstructed if we design sequences such that the corresponding FF  $G_{j,l}^{(p)}(\omega, T)$  has an odd component in the frequency domain.

In order to achieve this, it is necessary to better understand the structure of the balanced  $G^+$  filters. Observe that any function  $f(\omega)$  can be written as  $f(\omega) \equiv \mathcal{E}[f(\omega)] + \mathcal{O}[f(\omega)]$ ,

where its even and odd components are given, respectively, by

$$\mathcal{E}[f(\omega)] = \frac{f(\omega) + f(-\omega)}{2}, \quad \mathcal{O}[f(\omega)] = \frac{f(\omega) - f(-\omega)}{2}.$$

By manipulating the integral expressions of the  $G^+$  filters given in Eq. (20), we find

$$\begin{aligned} \mathcal{E}[G_{a,a';b,b'}^+(\omega, -\omega, T)] &= \int_{-T/2}^{T/2} ds \int_{-T/2}^{T/2} ds' \left\{ \mathcal{E}[y_{a,a'}(s + T/2)] \mathcal{E}[y_{b,b'}(s' + T/2)] \cos(\omega s) \cos(\omega s') \right. \\ &\quad \left. + \mathcal{O}[y_{b,b'}(s' + T/2)] \mathcal{O}[y_{a,a'}(s + T/2)] \sin(\omega s') \sin(\omega s) \right\}, \end{aligned} \quad (38)$$

$$\begin{aligned} \mathcal{O}[G_{a,a';b,b'}^+(\omega, -\omega, T)] &= i \int_{-T/2}^{T/2} ds \int_{-T/2}^{T/2} ds' \left\{ \mathcal{O}[y_{a,a'}(s + T/2)] \mathcal{E}[y_{b,b'}(s' + T/2)] \sin(\omega s) \cos(\omega s') \right. \\ &\quad \left. - \mathcal{O}[y_{b,b'}(s' + T/2)] \mathcal{E}[y_{a,a'}(s + T/2)] \sin(\omega s') \cos(\omega s) \right\}. \end{aligned} \quad (39)$$

From these expressions, it is evident that the even/odd character of the FFs can be traced back to the even/odd character of the switching functions  $y_{a,a'}(t + T/2)$  on  $[-T/2, T/2]$  or, equivalently, to the mirror symmetric/antisymmetric character of the switching functions on  $[0, T]$ . If the switching functions  $y_{a,a'}(s + T/2)$  and  $y_{b,b'}(s' + T/2)$  have the same parity (either both even or both odd), then the odd component of the FF vanishes. Conversely, if  $y_{a,a'}(s + T/2)$  and  $y_{b,b'}(s' + T/2)$  have opposite parity, the even component of the FF vanishes.

## B. A sample reconstruction

Finally, we combine all of the above tools and observations into a sample recipe for reconstructing the spectra influencing the qubit dynamics in the  $\Omega T \gg 1$  regime. **We consider a qubit with energy splitting  $\Omega/2\pi = 27$  GHz coupled to a bath that induces noise along all three axes of the Bloch sphere with non-negligible correlations between axes. In the Cartesian representation, we take the bath spectra to be sums of Gaussians centered at different locations in the frequency do-**

**main, given for all  $\alpha, \beta \in \{x, y, z\}$  by**

$$S_{\alpha,\beta}(\omega) = A_- e^{-\frac{(\omega-\omega_-)^2}{2\Delta^2}} + A_0 e^{-\frac{(\omega-\omega_0)^2}{2\Delta^2}} + A_+ e^{-\frac{(\omega-\omega_+)^2}{2\Delta^2}}. \quad (40)$$

If  $\omega_0 = 0$ ,  $\omega_- = -\omega_+$ , and  $A_+ = A_-$ , each  $S_{\alpha,\beta}(\omega)$  is an even function of  $\omega$ , symmetric about  $\omega = 0$ , indicating a classical noise source. For our simulations, we chose  $A_- = 332$  Hz,  $A_0 = 0.7A_-$ ,  $A_+ = 0.5A_-$ ,  $\Delta/2\pi = 0.80$  MHz,  $(\omega_{\mp} \pm \Omega)/2\pi = \pm 0.81$  MHz, and  $\omega_0/2\pi = 0.80$  MHz, which produce  $S_{\alpha,\beta}(\omega)$  that are *asymmetric* about  $\omega = 0$ , characteristic of quantum noise. In terms of the Cartesian spectra,  $S_{\pm 1, \mp 1}(\omega)$  are, in general, given by

$$S_{\pm 1, \mp 1}(\omega) = S_{x,x}(\omega) + S_{y,y}(\omega) \pm \text{Im}[S_{xy}(\omega)]. \quad (41)$$

Using Eq. (40) and our chosen simulation parameters, it is easy to see that  $S_{-1,+1}(-\Omega) \neq S_{+1,-1}(\Omega)$ , implying unequal emission and absorption rates.

Our objective is to reconstruct the dephasing spectrum  $S_{0,0}(\omega)$  and the spherical spectra  $S_{\pm 1, \mp 1}(\omega)$ , since they are the only dynamically relevant spectra in the  $\Omega T \gg 1$  regime. To accomplish this, we make use of the following six control sequences describing evolution over  $[0, T_c]$  in the interaction-picture frame,

$$\begin{aligned} U_1(0, T_c) &\equiv U_0\left(\frac{3T_c}{4}, T_c\right) [\pi]_z U_0\left(\frac{T_c}{4}, \frac{3T_c}{4}\right) [\pi]_z U_0\left(0, \frac{T_c}{4}\right), \\ U_2(0, T_c) &\equiv \left[\frac{\pi}{2}\right]_z U_0\left(\frac{3T_c}{4}, T_c\right) \left[\frac{\pi}{2}\right]_z U_0\left(\frac{T_c}{2}, \frac{3T_c}{4}\right) \left[\frac{\pi}{2}\right]_z U_0\left(\frac{T_c}{4}, \frac{T_c}{2}\right) \left[\frac{\pi}{2}\right]_z U_0\left(0, \frac{T_c}{4}\right), \\ U_3(0, T_c) &\equiv \left[\frac{3\pi}{2}\right]_z U_0\left(\frac{T_c}{2}, T_c\right) \left[\frac{\pi}{2}\right]_z U_0\left(0, \frac{T_c}{2}\right), \\ U_4(0, T_c) &\equiv [\pi]_z U_0\left(\frac{3T_c}{4}, T_c\right) [\pi]_y U_0\left(\frac{T_c}{2}, \frac{3T_c}{4}\right) [\pi]_z U_0\left(\frac{T_c}{4}, \frac{T_c}{2}\right) [\pi]_y U_0\left(0, \frac{T_c}{4}\right), \end{aligned}$$

$$\begin{aligned}
U_5(0, T_c) &\equiv [\pi]_x \tilde{U}_0\left(\frac{T_c}{2}, T_c\right) [\pi]_y \tilde{U}_0\left(\frac{T_c}{4}, \frac{T_c}{2}\right) [\pi]_z \tilde{U}_0\left(0, \frac{T_c}{4}\right), \\
U_6(0, T_c) &\equiv [\pi]_z \tilde{U}_0\left(\frac{3T_c}{4}, T_c\right) [\pi]_z \tilde{U}_0\left(\frac{T_c}{2}, \frac{3T_c}{4}\right) [\pi]_z \tilde{U}_0\left(\frac{T_c}{4}, \frac{T_c}{2}\right) [\pi]_z \tilde{U}_0\left(0, \frac{T_c}{4}\right).
\end{aligned}$$

Here,  $\tilde{U}_0(t_i, t_j) = [-\pi/4]_x U_0(t_i, t_j) [\pi/4]_x$  denotes free evolution in the interaction picture tilted by  $[\pi/4]_x$ , as described in Eq. (26). In addition to these sequences, the sample reconstruction relies on the quantities  $Q_1(T)$ ,  $Q_2(T)$ ,  $Q_3(T)$  and  $Q_4(T)$ . Using the approximate expressions in Eqs. (33)-(36), we obtain these quantities directly from expectation values of Pauli observables that we calculate numerically.

### 1. Sequences for reconstruction of $S_{\pm 1, \mp 1}(\omega)$

First, we detail the sequences and accessible quantities that we use to reconstruct the spherical spectra. Observe that by making a change of variable  $\omega \rightarrow \omega - \Omega$  in Eq. (37) and taking  $p = 1$ , the integrand of  $Q_1(T)$  depends on the product  $\mathcal{G}_{-1, +1}^{(1)}(\omega, T_c) S_{-1, +1}(\omega - \Omega)$ . To access  $\mathcal{E}[S_{-1, +1}(\omega - \Omega)]$  through  $Q_1(T)$ , we utilize the sequence  $U_1(0, T_c)$ , under which  $\mathcal{G}_{-1, +1}^{(1)}(\omega, T_c)$  is an even function of  $\omega$ , as shown in Fig. 1 (a). By applying  $M = 20$  repetitions of  $U_1(0, T_c)$  for different cycle times  $T_c = T_{\max}, T_{\max}/2, \dots, T_{\max}/8$  with  $T_{\max} = 2.4 \mu\text{s}$  and measuring  $Q_1(MT_c)$ , we produce 8 linear equations via the frequency comb approximation. Each of these equations contains terms of the form  $\mathcal{G}_{-1, +1}^{(1)}(n\omega_0, T_c) \mathcal{E}[S_{-1, +1}(n\omega_0 - \Omega)]$ , where  $n = 1, \dots, 8$  and  $\omega_0 = 2\pi/T_{\max}$ . While inverting this system is sufficient to reconstruct  $\mathcal{E}[S_{-1, +1}(\omega - \Omega)]$  at  $\omega = \omega_0, \dots, 8\omega_0$ , we cannot access this spectrum at  $\omega = 0$  since  $\mathcal{G}_{-1, +1}^{(1)}(0, T_c) = 0$  under  $U_1(0, T_c)$ . The sequence  $U_3(0, T_c)$ , on the other hand, has zero filter order, i.e.  $\mathcal{G}_{-1, +1}^{(1)}(0, T_c) \neq 0$ , as seen in Fig. 1 (c). Applying  $M = 20$  repetitions of  $U_3(0, T_c)$  for  $T_c = T_{\max}$  produces one additional linear equation that contains a term depending on  $\mathcal{G}_{-1, +1}^{(1)}(0, T_c) \mathcal{E}[S_{-1, +1}(-\Omega)]$ . Reconstructing  $\mathcal{O}[S_{-1, +1}(\omega - \Omega)]$  is impossible when  $\mathcal{G}_{-1, +1}^{(1)}(\omega, T_c)$  is an even function of  $\omega$ , as  $Q_1(T)$  will vanish. Instead, we rely on the sequence  $U_2(0, T_c)$  for which  $\mathcal{G}_{-1, +1}^{(1)}(\omega, T_c)$  is asymmetric about  $\omega = 0$ , depicted in Fig. 1 (b). Similar to the case of  $\mathcal{E}[S_{-1, +1}(\omega - \Omega)]$ , applying  $M = 20$  repetitions of  $U_2(0, T_c)$  for  $T_c = T_{\max}, T_{\max}/2, \dots, T_{\max}/8$  and measuring  $Q_1(MT_c)$ , produces 8 linear equations containing terms of the form  $\mathcal{G}_{-1, +1}^{(1)}(n\omega_0, T_c) \mathcal{O}[S_{-1, +1}(n\omega_0 - \Omega)]$ . It is not necessary to employ an additional sequence with zero filter order since  $\mathcal{O}[S_{-1, +1}(\omega - \Omega)]$ , being an odd function of  $\omega$ , vanishes at  $\omega = 0$ . Conveniently, we can access  $S_{+1, -1}(\omega)$  through quantity  $Q_2(T)$  using the same sequences. If we make the change of variable  $\omega \rightarrow \omega + \Omega$  in Eq. (37) and take  $p = 2$ , the integrand of  $Q_2(T)$  depends on  $\mathcal{G}_{+1, -1}^{(2)}(\omega, T_c) S_{+1, -1}(\omega + \Omega)$ . Analogous to the case of  $S_{-1, +1}(\omega)$ , measuring  $Q_2(MT_c)$  after applying  $M = 20$  repetitions of the sequences  $U_1(0, T_c)$  and  $U_2(0, T_c)$  for  $T_c = T_{\max}, T_{\max}/2, \dots, T_{\max}/8$

produces 8 linear equations containing the terms  $\mathcal{G}_{+1, -1}^{(2)}(n\omega_0, T_c) \mathcal{E}[S_{+1, -1}(n\omega_0 + \Omega)]$  and 8 linear equations containing the terms  $\mathcal{G}_{+1, -1}^{(2)}(n\omega_0, T_c) \mathcal{O}[S_{+1, -1}(n\omega_0 + \Omega)]$ , respectively, for  $n = 1, \dots, 8$ . As it requires a sequence with zero filter order, a linear equation involving  $\mathcal{G}_{+1, -1}^{(2)}(0, T_c) \mathcal{E}[S_{+1, -1}(\Omega)]$  is again obtained through  $U_3(0, T_c)$  with  $T_c = T_{\max}$ . The filters  $\mathcal{G}_{+1, -1}^{(2)}(\omega, T_c)$  generated by  $U_1(0, T_c)$ ,  $U_2(0, T_c)$  and  $U_3(0, T_c)$  are depicted in Fig. 1 (a-c). For each sequence, note that  $\mathcal{G}_{+1, -1}^{(2)}(\omega, T_c)$  is a reflection of its counterpart  $\mathcal{G}_{-1, +1}^{(2)}(\omega, T_c)$ .

### 2. Sequences for reconstruction of $S_{0,0}(\omega)$

The dephasing spectrum,  $S_{0,0}(\omega)$ , enters the qubit dynamics through  $Q_3(T)$  and  $Q_4(T)$  in Eq. (37). Note, however, that  $S_{\pm 1, \mp 1}(\omega)$  also enter  $Q_3(T)$  and  $Q_4(T)$ , a fact that prevents us from solving for the spherical and dephasing spectra individually. The filter  $\mathcal{G}_{0,0}^{(3)}(\omega, T_c)$ , which couples to  $S_{0,0}(\omega)$  in  $Q_3(T)$ , is an even function of  $\omega$  for sequence  $U_4(0, T_c)$ , as shown in Fig. 1 (d). Thus, measuring  $Q_3(T)$  after  $M = 20$  repetitions of  $U_4(0, T_c)$  for  $T_c = T_{\max}, T_{\max}/2, \dots, T_{\max}/8$  creates 8 linear equations that depend on  $\mathcal{G}_{0,0}^{(3)}(n\omega_0, T_c) \mathcal{E}[S_{0,0}(n\omega_0)]$ ,  $n = 1, \dots, 8$ .  $S_{0,0}(0)$  is extracted using  $U_6(0, T_c)$ , for which  $\mathcal{G}_{0,0}^{(3)}(0, T_c) \neq 0$ , as depicted in Fig. 1 (f). Applying  $M = 20$  repetitions of  $U_6(0, T_c)$  for  $T_c = T_{\max}$  generates an additional linear equation containing a term that depends on  $\mathcal{G}_{0,0}^{(3)}(0, T_c) \mathcal{E}[S_{0,0}(0)]$ . To access  $\mathcal{O}[S_{0,0}(n\omega_0)]$ , we must generate a filter that is not an even function of  $\omega$ . Under  $U_5(0, T_c)$ , the filter  $\mathcal{G}_{0,0}^{(4)}(\omega, T_c)$ , which couples to  $S_{0,0}(\omega)$  in  $Q_4(T)$ , is asymmetric about  $\omega = 0$  [Fig. 1 (e)]. Measuring  $Q_4(T)$  after  $M = 20$  repetitions of  $U_5(0, T_c)$  for  $T_c = T_{\max}, T_{\max}/2, \dots, T_{\max}/8$  creates 8 more linear equations containing terms  $\mathcal{G}_{0,0}^{(4)}(n\omega_0, T_c) \mathcal{O}[S_{0,0}(n\omega_0)]$ , for  $n = 1, \dots, 8$ , as needed.

### 3. Reconstruction results

To actually implement the reconstruction, we combine the linear equations generated in the previous steps (51 equations total, 17 for each spectrum). Inverting the system of equations produces estimates of  $\mathcal{E}[S_{\pm 1, \mp 1}(n\omega_0 \pm \Omega)]$  and  $\mathcal{E}[S_{0,0}(n\omega_0)]$  for  $n = 0, \dots, 8$ , as well as  $\mathcal{O}[S_{\pm 1, \mp 1}(n\omega_0 \pm \Omega)]$  and  $\mathcal{O}[S_{0,0}(n\omega_0)]$  for  $n = 1, \dots, 8$ . By combining the even and odd components of each spectrum, we obtain reconstructions of  $S_{\pm 1, \mp 1}(\omega)$  and  $S_{0,0}(\omega)$  in the frequency windows

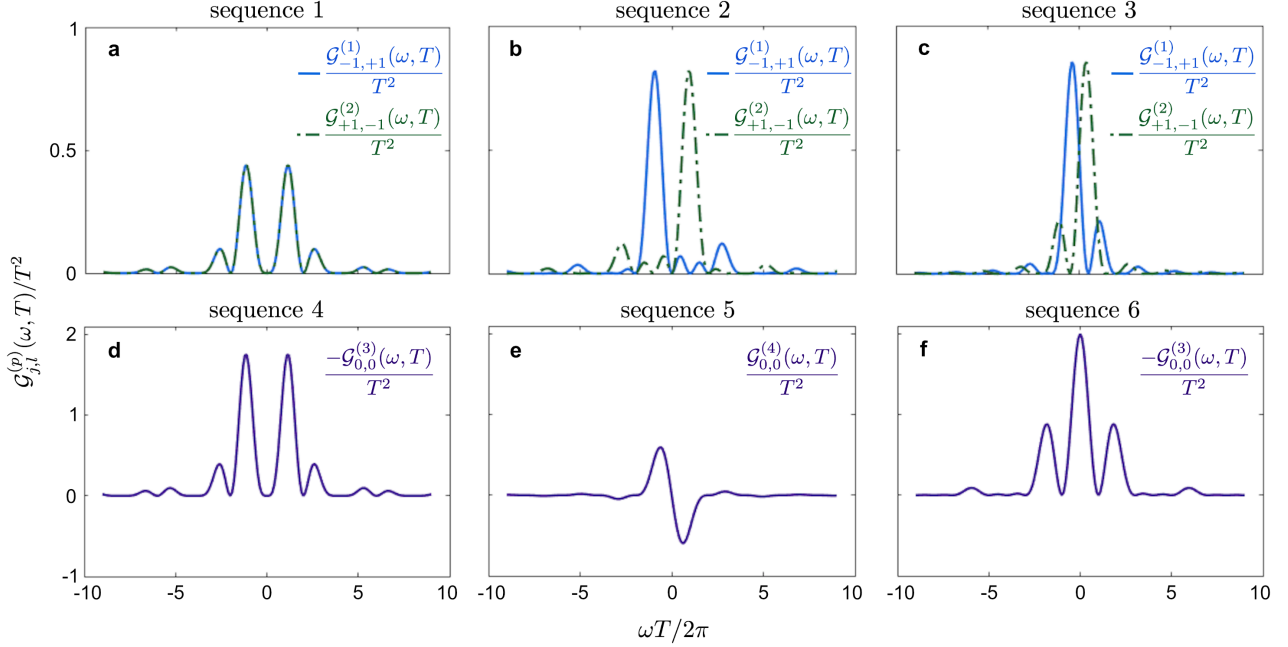


FIG. 1. (Color online) FFs used to reconstruct dynamically relevant spectra in the  $\Omega T \gg 1$  limit. Top: FFs used for the spherical spectra,  $S_{\pm 1, \mp 1}(\omega)$ . The FFs  $\mathcal{G}_{-1, +1}^{(1)}(\omega, T)$  (solid line) and  $\mathcal{G}_{+1, -1}^{(2)}(\omega, T)$  (dashed line), coupling to  $S_{-1, +1}(\omega)$  in  $Q_1(T)$  and  $S_{+1, -1}(\omega)$  in  $Q_2(T)$ , respectively, are plotted versus multiples of the harmonic frequency. Columns correspond to the control sequences  $U_1(0, T)$  (a),  $U_2(0, T)$  (b) and  $U_3(0, T)$  (c). Bottom: FFs used for the dephasing noise spectrum,  $S_{0,0}(\omega)$ . The FFs  $\mathcal{G}_{0,0}^{(3)}(\omega, T)$  and  $\mathcal{G}_{0,0}^{(4)}(\omega, T)$ , which couple to  $S_{0,0}(\omega)$  in  $Q_3(T)$  and  $Q_4(T)$ , respectively, are plotted versus multiples of the harmonic frequency. Columns correspond to the control sequences  $U_4(0, T)$  (d),  $U_5(0, T)$  (e) and  $U_6(0, T)$  (f). All FFs, top and bottom, are scaled by  $1/T^2$ , so that they are independent of  $T$ .

$[-8\omega_0 \pm \Omega, 8\omega_0 \pm \Omega]$  and  $[-8\omega_0, 8\omega_0]$ , respectively. Figure 2 shows plots of the actual and numerically reconstructed spectra in their respective windows. The remarkable accuracy of the reconstruction supports our formal claim in Sec. IV B 2 regarding the negligible contribution of certain spectra in the  $\Omega T \gg 1$  regime. The expectation values that we use to obtain  $Q_1(T)$ ,  $Q_2(T)$ ,  $Q_3(T)$  and  $Q_4(T)$  are calculated numerically using  $S_{\alpha, \beta}(\omega)$  in Eq. (40) for *all*  $\alpha, \beta$ . If there were dynamically relevant spectra besides  $S_{\pm 1, \mp 1}(\omega)$  and  $S_{0,0}(\omega)$ , significant deviations would have been observed.

Note that in our simulations we treated the qubit rotations that compose the sequences as being instantaneous in time. In a realistic implementation, this is a good approximation provided that the pulse-widths are much shorter than the free evolution time in the sequences. Staying within the regime of near instantaneous pulses places a lower limit on the amount of free evolution time and, hence, the cycle times  $T_c$ . This constrains the range over which the spectra can be reconstructed since the number of cycle times determines the number of sample points in the reconstruction. Leaving the regime of near instantaneous pulses will not affect the emergence of the frequency comb, though it can introduce distortions into the FFs. In principle, distortions arising from non-negligible pulse widths can be accounted for using the methods in [31].

## VI. LIMITATIONS OF COMB-BASED QNS

We conclude our present analysis by discussing an important practical limitation of the proposed QNS protocols, which is rooted in the frequency-comb approach. We do not intend this as a critique to the protocol itself, but, in the same spirit of recent work [44], as a way to highlight the regimes in which it is applicable under realistic conditions. We consider this to be crucial, as applying the protocol without being wary of the underlying assumptions may lead to misleading spectral reconstructions, as we demonstrate below.

As explained in Sec. III B, a key step in QNS protocols is ensuring the convolutions involving the filters and the spectra turn into discrete and, importantly, truncated sums (as in Eq. (23)). Once this is achieved, one can build a linear system of equations, from which the desired spectral information is extracted. In comb-based QNS protocols, this is achieved via the introduction of certain control symmetries – mainly sequence repetition, as it was the case in this paper. Crucially, the comb effectively generates a “sampling grid” in frequency, with points at multiples of a sampling frequency  $\omega_0 = 2\pi/T_c$ , which is fundamentally *upper-bounded* by the minimum achievable time resolution (finite in any experiment), and *lower-bounded* by the maximum possible evolution time (also necessarily finite). This mandates a physical upper bound on the sampling frequency.

As a result, issues arise when the target spectrum has a very wide support in frequency space. Imagine that the spectrum

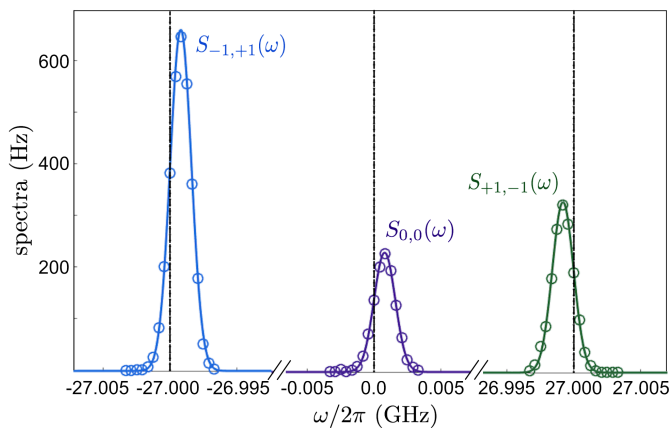


FIG. 2. (Color online) Reconstructions of target multi-axis spectra,  $\{S_{\mp 1, \pm 1}(\omega), S_{0,0}(\omega)\}$ , derived from Eq. (40). From left to right, the transverse noise spectrum  $S_{-1,+1}(\omega)$  (blue solid line) and reconstruction  $\hat{S}_{-1,+1}(\omega)$  (blue circles) are plotted in a frequency band centered at  $\omega = -\Omega$ , the dephasing noise spectrum  $S_{0,0}(\omega)$  (purple solid line) and reconstruction  $\hat{S}_{0,0}(\omega)$  (purple circles) are plotted in a frequency band centered at  $\omega = 0$ , and the transverse noise spectrum  $S_{+1,-1}(\omega)$  (green solid line) and reconstruction  $\hat{S}_{+1,-1}(\omega)$  (green circles) are plotted in a frequency band centered at  $\omega = \Omega$ . Dashed vertical lines, from left to right, correspond to the frequencies  $\omega = -\Omega$ ,  $\omega = 0$ , and  $\omega = \Omega$ .

has support in  $\omega \in [0, \Omega_{\text{cutoff}}]$ . The first step in a successful discretization is to guarantee that the convolution is well approximated by the discrete sum. This entails, as Eq. (23) suggests, that one has to guarantee that

$$K\omega_0 \geq \Omega_{\text{cutoff}},$$

namely, that the reconstruction window be *large enough to sample the full support/bandwidth of the spectrum*. Clearly, this implies that, given  $\Omega_{\text{cutoff}}$  and the upper bound on  $\omega_0$  implied by the physical constraints on the control, there is a lower bound,  $K_0$ , to the value of  $K$ , and thus on the size of the linear system of equations that may be assembled.

The problem arises when  $K_0$  is very large: this requires finding at least  $K_0$  sufficiently “different” control sequences that ensure the resulting linear system to be well-conditioned, thus affording a faithful and robust recovery of the desired spectral information. Since the FFs themselves decay with frequency, even though one may in principle displace the center of the filter in frequency, it becomes challenging to build a well-conditioned system of equations. This limitation has to be taken into account in designing the QNS protocol.

We stress that this is not an issue exclusive to multi-axis noise and, indeed, we tangentially discussed this question in a previous work [6], where we considered a pure-dephasing regime. However, in practical applications, and in particular in the context of solid-state devices, dephasing noise is typically associated with spectra that are strongly concentrated at low frequencies, which has proven to be favorable to comb-based QNS techniques. In both superconducting qubits and spin qubits, for instance, spectroscopy of dephasing noise has revealed spectra that are strongly suppressed with frequency,

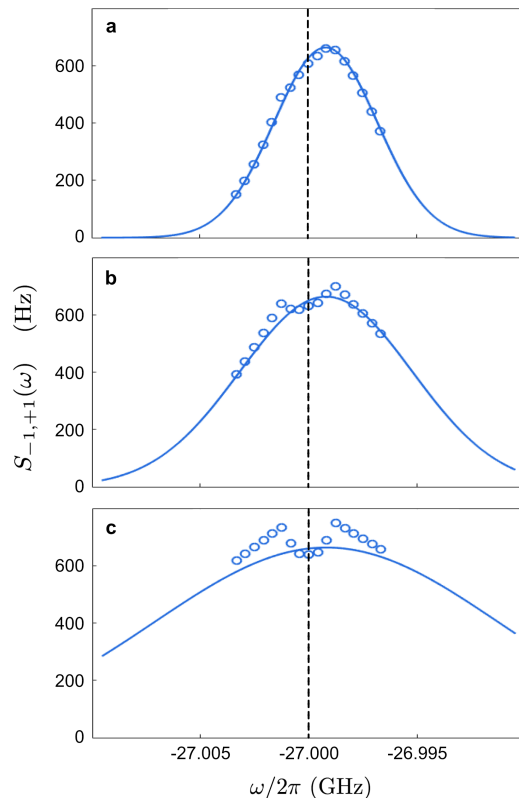


FIG. 3. (Color online) Effect of increased bandwidth. In a frequency band centered at  $\omega = -\Omega$ , three different transverse noise spectra (blue solid lines) are plotted along with their corresponding reconstructions (blue circles). The transverse spectra are Gaussian of varying bandwidth, with (a)  $\Delta/2\pi = 2.4$  MHz, (b)  $\Delta/2\pi = 4.0$  MHz, and (c)  $\Delta/2\pi = 8.0$  MHz.

typically following power-laws of the form  $\sim 1/\omega^{0.8-2.5}$ , arising from charge noise [25, 26], flux noise [2, 34], nuclear spin-baths [52], or external magnetic field instabilities [24]. By contrast, in these same systems, noise sources leading to qubit relaxation (here corresponding to noise along  $x$ ,  $y$ , or both) are commonly associated with spectra that *grow* with frequency, up to a cutoff that can be orders of magnitude above the qubit splitting. For example, for spin qubits in semiconductors, phononic environments play a prominent role in qubit relaxation [53–55], leading to spectra whose frequency dependencies correspond to rapidly increasing power laws [56]. Qubit-relaxation phenomena in the solid state also frequently involve Ohmic noise spectra ( $\propto \omega$ ). Examples of processes that can be associated with Ohmic spectra include Johnson-Nyquist noise afflicting spin qubits [55, 57], and two-level fluctuators coupled to superconducting qubits, for which a crossover between  $1/f$  and Ohmic noise is typically observed in the GHz frequency range [2, 23, 34, 58]. Comb-based QNS approaches are particularly ill-suited for such noise spectra; indeed, those techniques would then require including harmonics over a frequency support that can well be hundreds of GHz or more (up to the cutoff frequency), whereas the available control is rarely faster than 10 ns, leading to harmonics

separated by only  $\sim 100$  MHz. This would imply designing well-conditioned reconstructions including several thousands of pulse sequences. Therefore, we argue that the shortcomings of the comb approach described above will manifest themselves most strongly in a multi-axis setting, in which dephasing and relaxation noise are simultaneously characterized.

In order to showcase this effect more quantitatively, we fix the size of the reconstruction window and attempt to reconstruct spectra with increasingly large support in frequency space. The results, depicted in Fig. 3, show that as the support of the spectrum becomes larger, the quality of the reconstruction indeed decreases. More importantly, they support our previous warning: the choice of control sequences is dictated by the assumed width of the spectrum and this is an important consideration which has to be properly taken into account when implementing comb-based QNS protocols. These limitations can be potentially overcome, even in the general decoherence scenario, by switching to a more flexible continuous-time control paradigm (see Ref. [21] for a CW spectroscopy protocol in a dephasing-only regime). Developing and analyzing such improved protocols is one of the objectives of our current efforts [59].

## VII. CONCLUSION

We have presented a DD comb-based spectroscopy protocol capable of characterizing the noise affecting a qubit in all directions, i.e., a qubit undergoing general decoherence from a temporally correlated environment. This significantly increases our ability to understand, and eventually control, the different types of noise processes leading to corruption of information in a qubit, as we are now capable of simultaneously reconstructing the power spectra of noise inducing  $T_1$  and  $T_2$  processes, including their possible cross-correlations.

In particular, we showed how to extend comb-based noise spectroscopy methods to the general decoherence scenario for dynamical regimes of increasing complexity – from the simplest case where the internal qubit energy splitting  $\Omega$  is negligibly small, and only balanced filters enter the problem, similar in spirit to dephasing settings; to the practically relevant case where  $\Omega$  is large as compared to the inverse evolution time of the system, and the presence of imbalanced filters

mandates a qualitatively different treatment. The essence of our analysis is to recognize that, in each regime, *all the relevant power spectra can be accurately reconstructed* in principle. As a main result of independent interest, we have shown that, in the  $\Omega T \gg 1$  regime, these relevant spectra encompass a substantially smaller set than the original ones, consisting only of a dephasing spectrum and two (generally complex) transverse spherical spectra. In the process, we have provided constructive principles for control design, which allow the reconstruction of the target noise spectra to be carried out explicitly, as we have numerically demonstrated in a representative scenario.

In developing the proposed multi-axis noise spectroscopy protocol, we have purposefully restricted ourselves to control symmetries compatible with our previous results on comb-based spectroscopy of single-qubit non-Gaussian and multi-qubit Gaussian dephasing noise models [6, 41]. In principle, we expect that this should allow us to merge them with the results presented here in a relatively straightforward manner, thus achieving the coveted general multi-axis and multi-qubit noise characterization. This is part of our current efforts. On the experimental side, we expect that our results will be instrumental to further boost qubit fidelities, by paving the way to noise-tailored and noise-optimized quantum control modalities. Indeed, subject to the caveats we elucidated in Sec. VI in relation to spectra with extended bandwidth, similar experiments to the ones performed in platforms where dephasing noise is dominant [24, 26, 31], should now also be possible in platforms where both  $T_1$  and  $T_2$  processes are significant. As we already mentioned, we intend to separately address the challenge posed by extended spectral support, by turning to continuous control modulation [59].

## ACKNOWLEDGEMENTS

This research was funded by the U.S. Army Research Office grant No. W911NF-141-0682, the U.S. MURI grant No. W911NF1810218 (to L.V.), the AUSMURI grant No. AUSMURI000002 and the DECRA fellowship DE170100088 (to G.P.S.). F.B. also gratefully acknowledges support from the *Fonds de Recherche du Québec-Nature et Technologies*.

## Appendix A: Accessible quantities for vanishing qubit splitting

In Sec. IV A of the main text, we showed that only  $G^+$  filters are necessary for QNS protocols. This need not imply, however, that  $G^-$  filters do not contribute to the reduced qubit dynamics. Indeed, an explicit calculation shows that, in general, both types

of filters can contribute. We find:

$$\begin{aligned}
C_{x,0} &= -2 \int_0^\infty \frac{d\omega}{2\pi} (\text{Re}[S_{y,y}^+(\omega)]\text{Re}[G_{y,y,y,y}^+(\omega, T)] + \text{Re}[S_{z,z}^+(\omega)]\text{Re}[G_{z,z,z,z}^+(\omega, T)]), \\
C_{y,0} &= -2 \int_0^\infty \frac{d\omega}{2\pi} (\text{Re}[S_{x,x}^+(\omega)]\text{Re}[G_{x,x,x,x}^+(\omega, T)] + \text{Re}[S_{z,z}^+(\omega)]\text{Re}[G_{z,z,z,z}^+(\omega, T)]), \\
C_{z,0} &= -2 \int_0^\infty \frac{d\omega}{2\pi} (\text{Re}[S_{x,x}^+(\omega)]\text{Re}[G_{x,x,x,x}^+(\omega, T)] + \text{Re}[S_{z,z}^+(\omega)]\text{Re}[G_{z,z,z,z}^+(\omega, T)]), \\
C_{x,y} - C_{z,y} &= 4i \int_0^\infty \frac{d\omega}{2\pi} (\text{Im}[S_{x,z}^+(\omega)]\text{Im}[G_{x,x,z,z}^+(\omega, T)] - \text{Re}[S_{x,z}^+(\omega)]\text{Re}[G_{x,x,z,z}^+(\omega, T)]), \\
C_{x,z} - C_{y,z} &= -4i \int_0^\infty \frac{d\omega}{2\pi} (\text{Im}[S_{x,y}^+(\omega)]\text{Im}[G_{x,x,y,y}^+(\omega, T)] - \text{Re}[S_{x,y}^+(\omega)]\text{Re}[G_{x,x,y,y}^+(\omega, T)]), \\
C_{z,x} - C_{y,x} &= 4i \int_0^\infty \frac{d\omega}{2\pi} (\text{Im}[S_{y,z}^+(\omega)]\text{Im}[G_{y,y,z,z}^+(\omega, T)] - \text{Re}[S_{y,z}^+(\omega)]\text{Re}[G_{y,y,z,z}^+(\omega, T)]), \\
C_{x,y} + C_{z,y} &= -4i \int_0^\infty \frac{d\omega}{2\pi} (\text{Im}[S_{x,z}^+(\omega)]\text{Im}[G_{x,x,z,z}^-(\omega, T)] - \text{Re}[S_{x,z}^+(\omega)]\text{Re}[G_{x,x,z,z}^-(\omega, T)]), \\
C_{x,z} + C_{y,z} &= 4i \int_0^\infty \frac{d\omega}{2\pi} (\text{Im}[S_{x,y}^+(\omega)]\text{Im}[G_{x,x,y,y}^-(\omega, T)] - \text{Re}[S_{x,y}^+(\omega)]\text{Re}[G_{x,x,y,y}^-(\omega, T)]), \\
C_{z,x} + C_{y,x} &= 4i \int_0^\infty \frac{d\omega}{2\pi} (\text{Im}[S_{y,z}^+(\omega)]\text{Im}[G_{y,y,z,z}^-(\omega, T)] - \text{Re}[S_{y,z}^+(\omega)]\text{Re}[G_{y,y,z,z}^-(\omega, T)]), \\
C_{x,x} &= 4 \int_0^\infty \frac{d\omega}{2\pi} (\text{Re}[S_{y,z}^-(\omega)]\text{Im}[G_{y,y,z,z}^+(\omega, T)] + \text{Im}[S_{y,z}^-(\omega)]\text{Re}[G_{y,y,z,z}^+(\omega, T)]), \\
C_{y,y} &= 4 \int_0^\infty \frac{d\omega}{2\pi} (\text{Re}[S_{x,z}^-(\omega)]\text{Im}[G_{x,x,z,z}^+(\omega, T)] + \text{Im}[S_{x,z}^-(\omega)]\text{Re}[G_{x,x,z,z}^+(\omega, T)]), \\
C_{z,z} &= 4 \int_0^\infty \frac{d\omega}{2\pi} (\text{Re}[S_{x,y}^-(\omega)]\text{Im}[G_{x,x,y,y}^+(\omega, T)] + \text{Im}[S_{x,y}^-(\omega)]\text{Re}[G_{x,x,y,y}^+(\omega, T)]).
\end{aligned}$$

As one can see from the above equations, by also recalling Eq. (27), the expectation value of any observable, given an arbitrary initial state, manifestly depends on both  $G^+$  and  $G^-$  filters in general. What makes the multi-axis dynamics special is that one may identify combinations of observable-and-initial state, which depend solely on  $G^+$  filters – in stark contrast to a multiqubit scenario under pure dephasing [41].

### Appendix B: On the vanishing of imbalanced filters in the large $\Omega T$ regime

In Sec. IV B 2 of the main text, we provided the intuition behind the observation that, when the splitting  $\Omega$  is sufficiently large, certain filters and the corresponding spectra do not contribute to the probe dynamics. Here we show this more formally.

To see the argument in detail, note that the filters  $G^\pm$  are linear combinations of the second-order filters  $F_{a,a';b,b'}^{(2)}(\omega + s\Omega, -\omega + s'\Omega, T)$ . The filter is balanced when  $s + s' = 0$  and imbalanced otherwise (whenever  $s + s' = \pm 1$  or  $s + s' = \pm 2$ ). By redefining the integration variables in terms of  $t_\pm \equiv (t_1 \pm t_2)/2$ , it follows then that we can rewrite the filter as

$$F_{a,a';b,b'}^{(2)}(\omega + s\Omega, -\omega + s'\Omega, T)/2 = \int_{\Lambda_\pm} d\vec{t} e^{i[2\omega + (s-s')\Omega]t_- + i(s+s')\Omega t_+} y_{a,a'}(t_+ + t_-) y_{b,b'}(t_+ - t_-), \quad (\text{B1})$$

where  $\Lambda_\pm$  is the triangular integration domain defined by the vertices  $\{(t_-, t_+)\} = \{(0, T), (T/2, T/2), (0, 0)\}$  or, alternatively, by the relations  $t_- \in [0, T/2]$  and  $t_+ \in [t_-, T - t_-]$ . Let us further assume that the applied control induced switching functions are ‘‘slow’’ compared to  $\Omega$ . That is to say, we assume that  $y_{c,c'}(t_\pm \pm t_\mp)$ , for  $c, c' = a, b$ , is well approximated by its truncated inverse Fourier transform, namely,

$$y_{c,c'}(t_\pm \pm t_\mp) \simeq \int_{-\Omega_0}^{\Omega_0} \frac{d\omega_\pm^{(\bar{c})}}{2\pi} e^{i\omega_\pm^{(\bar{c})}t_\pm} \int_{-\Omega_0}^{\Omega_0} \frac{d\omega_\mp^{(\bar{c})}}{2\pi} e^{i\omega_\mp^{(\bar{c})}t_\mp} \hat{y}_{c,c'}^\pm(\omega_\pm^{(\bar{c})}, \omega_\mp^{(\bar{c})}),$$

where  $\hat{y}_{c,c'}^\pm(\omega_+^{(\vec{c})}, \omega_-^{(\vec{c})})$  represents the Fourier transform of  $y_{c,c'}(t_+ \pm t_-)$  and  $\Omega_0 \ll \Omega$  is the integration bound. By using this expression to rewrite  $y_{a,a'}(t_+ + t_-)$  and  $y_{b,b'}(t_+ - t_-)$ , the FF in Eq. (B1) becomes

$$F_{a,a';b,b'}^{(2)}(\omega + s\Omega, -\omega + s'\Omega, T)/2 = \mathcal{I}(o_+, o_-) \hat{y}_{a,a'}^+(\omega_+^{(\vec{a})}, \omega_-^{(\vec{a})}) \hat{y}_{b,b'}^-(\omega_+^{(\vec{b})}, \omega_-^{(\vec{b})}),$$

where

$$\mathcal{I}(o_+, o_-) \equiv \int_{\Lambda_\pm} d\vec{t} e^{it_+o_+} e^{it_-o_-}, \quad o_- \equiv 2\omega + (s - s')\Omega - (\omega_-^{(\vec{a})} + \omega_-^{(\vec{b})}), \quad o_+ \equiv (s + s')\Omega - (\omega_+^{(\vec{a})} + \omega_+^{(\vec{b})}). \quad (\text{B2})$$

By letting  $\alpha = o_+/o_-$ , substituting  $o_- = (1/\alpha)o_+$  into  $\mathcal{I}(o_+, o_-)$ , and performing the time integration, we find

$$|\mathcal{I}(o_+, o_-)| \leq \begin{cases} \frac{T^2}{(o_+T)^2} \left( \left| \frac{\alpha}{1+\alpha} \right| + \left| \frac{2\alpha^2}{-1+\alpha^2} \right| + \left| \frac{\alpha}{-1+\alpha} \right| \right), & \alpha \neq 1, \\ T^2 \left( \frac{1}{(o_+T)^2} + \left| \frac{1}{2o_+T} \right| \right), & \alpha = 1. \end{cases}$$

From this expression, it is apparent that  $|\mathcal{I}(o_+, o_-)|$  and, hence,  $|F_{a,a';b,b'}^{(2)}(\omega + s\Omega, -\omega + s'\Omega, T)|$ , are small whenever  $|o_+T| \gg 1$ .

To verify that this condition is met, recall that  $|\omega_+^{(\vec{a})}|, |\omega_+^{(\vec{b})}| \leq \Omega_0 \ll \Omega$  due to our assumption of slow control. From Eq. (B2), it then follows that  $|o_+| \geq |s + s'|\Omega - 2\Omega_0$ . This translates into the observation that whenever

$$T|o_+| \geq T \left| |s + s'|\Omega - 2\Omega_0 \right| \gg 1,$$

the contributions from imbalanced filters are negligible compared to those of balanced filters, for both  $G^+$  and  $G^-$ . Since  $\Omega \gg \Omega_0$  by the assumption of slow control, we can practically neglect the imbalanced filters whenever  $\Omega T \gg 1$ .

- 
- [1] J. P. Dowling and G. J. Milburn, “Quantum technology: the second quantum revolution,” *Phil. Trans. R. Soc. London A* **361**, 1655 (2003).
- [2] J. Bylander, S. Gustavsson, F. Yan, F. Yoshihara, K. Harrabi, G. Fitch, D. G. Cory, Y. Nakamura, J.-S. Tsai, and W. D. Oliver, “Noise spectroscopy through dynamical decoupling with a superconducting flux qubit,” *Nat. Phys.* **7**, 565 (2011).
- [3] G. A. Álvarez and D. Suter, “Measuring the spectrum of colored noise by dynamical decoupling,” *Phys. Rev. Lett.* **107**, 230501 (2011).
- [4] I. Almog, Y. Sagi, G. Gordon, G. Bensky, G. Kurizki, and N. Davidson, “Direct measurement of the system–environment coupling as a tool for understanding decoherence and dynamical decoupling,” *J. Phys. B* **44**, 154006 (2011).
- [5] L. M. Norris, D. Lucarelli, V. M. Frey, S. Mavadia, M. J. Biercuk, and L. Viola, “Optimally band-limited spectroscopy of control noise using a qubit sensor,” *Phys. Rev. A* **98**, 032315 (2018).
- [6] L. M. Norris, G. A. Paz-Silva, and L. Viola, “Qubit noise spectroscopy for non-Gaussian dephasing environments,” *Phys. Rev. Lett.* **116**, 150503 (2016).
- [7] C. Ferrie, C. Granade, G. A. Paz-Silva, and H. M. Wiseman, “Bayesian quantum noise spectroscopy,” *New J. Phys.* **20**, 123005 (2018).
- [8] P. Wang, C. Chen, X. Peng, J. Wrachtrup, and R.-B. Liu, “Characterization of arbitrary-order correlations in quantum baths by weak measurement,” arXiv:1902.03606 (2019).
- [9] K. Temme, S. Bravyi, and J. M. Gambetta, “Error mitigation for short-depth quantum circuits,” *Phys. Rev. Lett.* **119**, 180509 (2017).
- [10] S. Endo, S. C. Benjamin, and Y. Li, “Practical quantum error mitigation for near-future applications,” *Phys. Rev. X* **8**, 031027 (2018).
- [11] J. Preskill, “Quantum computing in the NISQ era and beyond,” *Quantum* **2**, 79 (2018).
- [12] J. Preskill, “Sufficient condition on noise correlations for scalable quantum computing,” *Quantum Inf. Comput.* **13**, 181 (2013).
- [13] F. Beaudoin, L. M. Norris, and L. Viola, “Ramsey interferometry in correlated quantum noise environments,” *Phys. Rev. A* **98**, 020102(R) (2018).
- [14] F. Yan, D. Campbell, P. Krantz, M. Kjaergaard, D. Kim, J. L. Yoder, D. Hover, A. Sears, A. J. Kerman, T. P. Orlando, S. Gustavsson, and W. D. Oliver, “Distinguishing coherent and thermal photon noise in a circuit quantum electrodynamical system,” *Phys. Rev. Lett.* **120**, 260504 (2018).
- [15] U. von Lüpké, F. Beaudoin, L. M. Norris, Y. Sung, R. Winik, J. Y. Qiu, M. Kjaergaard, D. Kim, J. Yoder, S. Gustavsson, L. Viola, and W. D. Oliver, “Two-qubit spectroscopy of spatiotemporally correlated quantum noise in superconducting qubits,” forthcoming (2019).
- [16] Y.-Q. Chen, K.-L. Ma, Y.-C. Zheng, J. Allcock, S. Zhang, and C.-Y. Hsieh, “Non-Markovian noise characterization with the transfer tensor method,” arXiv:1905.10941 (2019).
- [17] S. Gustavsson, J. Bylander, F. Yan, W. D. Oliver, F. Yoshihara, and Y. Nakamura, “Noise correlations in a flux qubit with tunable tunnel coupling,” *Phys. Rev. B* **84**, 014525 (2011).
- [18] T. Yuge, S. Sasaki, and Y. Hirayama, “Measurement of the noise spectrum using a multiple-pulse sequence,” *Phys. Rev. Lett.* **107**, 170504 (2011).

- [19] P. Szankowski, G. Ramon, J. Krzywda, D. Kwiatkowski, and Ł. Cywiński, “Environmental noise spectroscopy with qubits subjected to dynamical decoupling,” *J. Phys.: Cond. Matter* **29**, 333001 (2017).
- [20] F. Yan, S. Gustavsson, J. Bylander, X. Jin, F. Yoshihara, D. G. Cory, Y. Nakamura, T. P. Orlando, and W. D. Oliver, “Rotating-frame relaxation as a noise spectrum analyser of a superconducting qubit undergoing driven evolution,” *Nat. Commun.* **4**, 2337 (2013).
- [21] K. Willick, D. K. Park, and J. Baugh, “Efficient continuous-wave noise spectroscopy beyond weak coupling,” *Phys. Rev. A* **98**, 013414 (2018).
- [22] M. J. Biercuk, A. C. Doherty, and H. Uys, “Dynamical decoupling sequence construction as a filter-design problem,” *J. Phys. B* **44**, 154002 (2011).
- [23] C. M. Quintana, Yu Chen, D. Sank, A. G. Petukhov, T. C. White, D. Kafri, B. Chiaro, A. Megrant, R. Barends, B. Campbell, Z. Chen, A. Dunsworth, A. G. Fowler, R. Graff, E. Jeffrey, J. Kelly, E. Lucero, J. Y. Mutus, M. Neeley, C. Neill, P. J. J. O’Malley, P. Roushan, A. Shabani, V. N. Smelyanskiy, A. Vainsencher, J. Wenner, H. Neven, and J. M. Martinis, “Observation of classical-quantum crossover of  $1/f$  flux noise and its paramagnetic temperature dependence,” *Phys. Rev. Lett.* **118**, 057702 (2017).
- [24] J. T. Muhonen, J. P. Dehollain, A. Laucht, F. E. Hudson, R. Kalra, T. Sekiguchi, K. M. Itoh, D. N. Jamieson, J. C. McCallum, A. S. Dzurak, and A. Morello, “Storing quantum information for 30 seconds in a nanoelectronic device,” *Nat. Nanotechnol.* **9**, 986 (2014).
- [25] J. Yoneda, K. Takeda, T. Otsuka, T. Nakajima, M. R. Delbecq, G. Allison, T. Honda, T. Kodera, S. Oda, Y. Hoshi, N. Usami, K.M. Itoh, and S. Tarucha, “A quantum-dot spin qubit with coherence limited by charge noise and fidelity higher than 99.9%,” *Nat. Nanotechnol.* **13**, 102 (2018).
- [26] K. W. Chan, W. Huang, C. H. Yang, J. C. C. Hwang, B. Hensen, T. Tanttu, F. E. Hudson, K. M. Itoh, A. Laucht, A. Morello, and A. S. Dzurak, “Assessment of a silicon quantum dot spin qubit environment via noise spectroscopy,” *Phys. Rev. Applied* **10**, 044017 (2018).
- [27] S. Kotler, N. Akerman, Y. Glickman, and R. Ozeri, “Nonlinear single-spin spectrum analyzer,” *Phys. Rev. Lett.* **110**, 110503 (2013).
- [28] Y. Wang, M. Um, J. Zhang, S. An, M. Lyu, J.-N. Zhang, L.-M. Duan, D. Yum, and K. Kim, “Single-qubit quantum memory exceeding ten-minute coherence time,” *Nature Photonics* **11**, 646 (2017).
- [29] N. Bar-Gill, L. M. Pham, C. Belthangady, D. Le Sage, P. Cappellaro, J. R. Maze, M. D. Lukin, A. Yacoby, and R. Walsworth, “Suppression of spin-bath dynamics for improved coherence of multi-spin-qubit systems,” *Nat. Commun.* **3**, 858 (2012).
- [30] S. Hernández-Gómez, F. Poggiali, P. Cappellaro, and N. Fabbrì, “Noise spectroscopy of a quantum-classical environment with a diamond qubit,” *Phys. Rev. B* **98**, 214307 (2018).
- [31] Y. Sung, F. Beaudoin, L. M. Norris, F. Yan, D. K. Kim, J. Y. Qiu, U. von Lüepke, J. L. Yoder, T. P. Orlando, S. Gustavsson, L. Viola, and W. D. Oliver, “Non-Gaussian noise spectroscopy with a superconducting qubit sensor,” *Nat. Commun.* **10**, 3715 (2019).
- [32] J. A. Schreier, A. A. Houck, J. Koch, D. I. Schuster, B. R. Johnson, J. M. Chow, J. M. Gambetta, J. Majer, L. Frunzio, M. H. Devoret, S. M. Girvin, and R. J. Schoelkopf, “Suppressing charge noise decoherence in superconducting charge qubits,” *Phys. Rev. B* **77**, 180502 (2008).
- [33] R. Barends, J. Kelly, A. Megrant, D. Sank, E. Jeffrey, Y. Chen, Y. Yin, B. Chiaro, J. Mutus, C. Neill, P. O’Malley, P. Roushan, J. Wenner, T. C. White, A. N. Cleland, and J. M. Martinis, “Coherent Josephson qubit suitable for scalable quantum integrated circuits,” *Phys. Rev. Lett.* **111**, 080502 (2013).
- [34] F. Yan, S. Gustavsson, A. Kamal, J. Birenbaum, A. P. Sears, D. Hover, T. J. Gudmundsen, D. Rosenberg, G. Samach, S. Weber, J. L. Yoder, T. P. Orlando, J. Clarke, A. J. Kerman, and W. D. Oliver, “The flux qubit revisited to enhance coherence and reproducibility,” *Nat. Commun.* **7**, 12964 (2016).
- [35] X. Mi, M. Benito, S. Putz, D. M. Zajac, J. M. Taylor, G. Burkard, and J. R. Petta, “A coherent spin–photon interface in silicon,” *Nature* **555**, 599 (2018).
- [36] A. J. Landig, J. V. Koski, P. Scarlino, U. C. Mendes, A. Blais, C. Reichl, W. Wegscheider, A. Wallraff, K. Ensslin, and T. Ihn, “Coherent spin–photon coupling using a resonant exchange qubit,” *Nature* **560**, 179 (2018).
- [37] A. Kha, R. Joynt, and D. Culcer, “Do micromagnets expose spin qubits to charge and Johnson noise?” *Appl. Phys. Lett.* **107**, 172101 (2015).
- [38] M. Russ, F. Ginzler, and G. Burkard, “Coupling of three-spin qubits to their electric environment,” *Phys. Rev. B* **94**, 165411 (2016).
- [39] F. Beaudoin, D. Lachance-Quirion, W. A. Coish, and M. Pioro-Ladrière, “Coupling a single electron spin to a microwave resonator: controlling transverse and longitudinal couplings,” *Nanotech.* **27**, 464003 (2016).
- [40] P. Szańkowski, M. Trippenbach, and Ł. Cywiński, “Spectroscopy of cross-correlations of environmental noises with two qubits,” *Phys. Rev. A* **94**, 012109 (2016).
- [41] G. A. Paz-Silva, L. M. Norris, and L. Viola, “Multiqubit spectroscopy of Gaussian quantum noise,” *Phys. Rev. A* **95**, 022121 (2017).
- [42] J. Krzywda, P. Szańkowski, and Ł. Cywiński, “The dynamical-decoupling-based spatiotemporal noise spectroscopy,” *New J. Phys.* **21**, 043034 (2019).
- [43] G. A. Paz-Silva and L. Viola, “General transfer-function approach to noise filtering in open-loop quantum control,” *Phys. Rev. Lett.* **113**, 250501 (2014).
- [44] P. Szańkowski and Ł. Cywiński, “Accuracy of dynamical-decoupling-based spectroscopy of Gaussian noise,” *Phys. Rev. A* **97**, 032101 (2018).
- [45] L. Viola, S. Lloyd, and E. Knill, “Universal control of decoupled quantum systems,” *Phys. Rev. Lett.* **83**, 4888 (1999).
- [46] We remark that the separation into  $H_S$  and  $H_{SB}$  in Eq. (1) is dictated by the problem and task at hand. If the external control Hamiltonian supplies full qubit controllability, one can formally redefine  $H_{SB}$  to also include  $H_S$ . On the other hand, in several physical systems of interest,  $H_S$  is necessary to achieve full qubit controllability and cannot be included in  $H_{SB}$ .
- [47] Formally, we are demanding that the system-bath coupling, the controls being used, and the relevant spectra, are such that the (operator) norm  $\|\sum (-i)^k \mathcal{C}^{(k)} / k!\| \simeq \|-i\mathcal{C}^{(1)} - \mathcal{C}^{(2)}/2\|$ . For instance, this will be appropriate in a weak-coupling regime, as discussed e.g. in [51].
- [48] V. M. Frey, S. Mavadia, L. M. Norris, W. de Ferranti, D. Lucarelli, and L. Viola, “Application of optimal band-limited control protocols to quantum noise sensing,” *Nat. Commun.* **8**, 2189 (2017).
- [49] A. A. Clerk, M. H. Devoret, S. M. Girvin, F. Marquardt, and R. J. Schoelkopf, *Rev. Mod. Phys.* **82**, 1155 (2010).
- [50] G. A. Paz-Silva, S.-W. Lee, T. J. Green, and L. Viola, “Dynamical decoupling sequences for multi-qubit dephasing suppression and long-time quantum memory,” *New J. Phys.* **18**, 073020 (2016).

- [51] H.-P. Breuer and F. Petruccione, *The Theory of Open Quantum Systems* (Oxford University Press, Oxford, 2002).
- [52] F. K. Malinowski, F. Martins, Ł. Cywiński, M. S. Rudner, P. D. Nissen, S. Fallahi, G. C. Gardner, M. J. Manfra, C. M. Marcus, and F. Kuemmeth, “Spectrum of the nuclear environment for gas spin qubits,” *Phys. Rev. Lett.* **118**, 177702 (2017).
- [53] T. Meunier, I. T. Vink, L. H. Willems van Beveren, K.-J. Tielrooij, R. Hanson, F. H. L. Koppens, H. P. Tranitz, W. Wegscheider, L. P. Kouwenhoven, and L. M. K. Vandersypen, “Experimental signature of phonon-mediated spin relaxation in a two-electron quantum dot,” *Phys. Rev. Lett.* **98**, 126601 (2007).
- [54] C. H. Yang, A. Rossi, R. Ruskov, N. S. Lai, F. A. Mohiyaddin, S. Lee, C. Tahan, G. Klimeck, A. Morello, and A. S. Dzurak, “Spin-valley lifetimes in a silicon quantum dot with tunable valley splitting,” *Nat. Commun.* **4**, 2069 (2013).
- [55] L. Petit, J. M. Boter, H. G. J. Eenink, G. Droulers, M. L. V. Tagliaferri, R. Li, D. P. Franke, K. J. Singh, J. S. Clarke, R. N. Schouten, V. V. Dobrovitski, L. M. K. Vandersypen, and M. Veldhorst, “Spin lifetime and charge noise in hot silicon quantum dot qubits,” *Phys. Rev. Lett.* **121**, 076801 (2018).
- [56] C. Tahan and R. Joynt, “Relaxation of excited spin, orbital, and valley qubit states in ideal silicon quantum dots,” *Phys. Rev. B* **89**, 075302 (2014).
- [57] P. Huang and X. Hu, “Electron spin relaxation due to charge noise,” *Phys. Rev. B* **89**, 195302 (2014).
- [58] A. Shnirman, G. Schön, I. Martin, and Y. Makhlin, “Low- and high-frequency noise from coherent two-level systems,” *Phys. Rev. Lett.* **94**, 127002 (2005).
- [59] L. M. Norris, G. A. Paz-Silva, F. Beaudoin, and L. Viola, “Spectral estimation of multi-axis quantum noise by continuous control modulation,” forthcoming (2019).